Synoptic Analysis and Hindcast of an Intense Bow Echo in Western Europe: The 9 June 2014 Storm

LUCA MATHIAS, VOLKER ERMERT, FANNI D. KELEMEN,[a] AND PATRICK LUDWIG

Institute for Geophysics and Meteorology, University of Cologne, Cologne, Germany

JOAQUIM G. PINTO

Department of Meteorology, University of Reading, Reading, United Kingdom, and Institute of Meteorology and Climate Research, Karlsruhe Institute of Technology, Karlsruhe, Germany

ABSTRACT

On Pentecost Monday, 9 June 2014, a severe linearly organized mesoscale convective system (MCS) hit Belgium and western Germany. This storm was one of the most severe thunderstorms in Germany in decades. The synoptic scale and mesoscale characteristics of this storm are analyzed based on remote sensing data and in situ measurements. Moreover, the forecast potential of the storm is evaluated using sensitivity experiments with a regional climate model. The key ingredients for the development of the Pentecost storm were the concurrent presence of low level moisture, atmospheric conditional instability, and wind shear. The synoptic and mesoscale analysis shows that the outflow of a decaying MCS above northern France triggered the storm, which exhibited the typical features of a bow echo like a bookend vortex and a rear inflow jet. This resulted in hurricane force wind gusts (reaching 40 m s $^{-1}$) along a narrow swath in the Rhine Ruhr region leading to substantial damage. Operational numerical weather prediction models mostly failed to forecast the storm, but high resolution regional model hindcasts enable a realistic simulation of the storm. The model experiments reveal that the development of the bow echo is particularly sensitive to the initial wind field and the lower tropospheric moisture content. Adequate initial and boundary conditions are therefore essential for realistic numerical forecasts of such a bow echo event. It is concluded that the Pentecost storm exhibited a comparable structure and a similar intensity to observed bow echo systems in the United States.

1. Introduction

On Pentecost Monday, 9 June 2014, a well-organized convective system crossed over Belgium and the northwestern part of Germany, causing severe wind damage along its path, particularly in the federal state of North Rhine Westphalia (NRW). Short-term warnings based on nowcasting were issued for NRW and widespread severe weather was observed over the Rhine Ruhr area (Fig. 1). Maximum wind gusts reached about 40 m s $^{-1}$ at the Düsseldorf Airport in Germany, which had to be temporarily closed. Within Düsseldorf's periphery, nearly one-third of all roadside trees were heavily damaged. Moreover, rail traffic was severely disrupted in NRW (see Fig. 1) as a result of the large number of overturned trees. In addition to the wind gusts and heavy precipitation, localized hail bursts were reported across the area (Fig. 1). During this event, six fatalities, more than 50 casualties, and total insured losses of about 650 million euros were reported (Deutsche Rück 2015). The German Weather Service [Deutscher Wetterdienst (DWD)] attributed to this warm-season severe wind event an approximate return period of more than 50 yr for Germany (Beyer and Tuschy 2015). These specific characteristics motivated a detailed investigation of this event, hereafter referred to as the Pentecost storm.

Mesoscale convective systems (MCSs) occur more frequently during the summer months and can produce hazardous weather events, such as flash floods, large hail, and storm-force wind gusts that can occasionally reach hurricane-force levels. Wind gusts accompanying MCSs are induced by strong downdrafts and by the

[a] Current affiliation: Institute of Meteorology and Climate Research, Karlsruhe Institute of Technology, Karlsruhe, Germany.

Corresponding author: Luca Mathias, mathiasl@smail.uni koeln.de

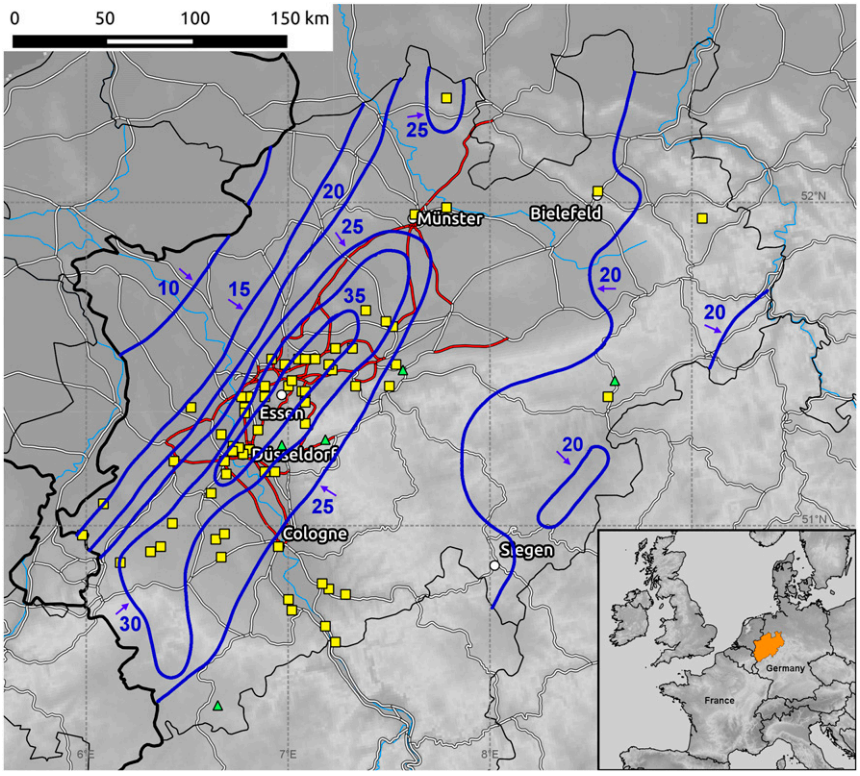

FIG. 1. Illustration of the observed damage in NRW during the passage of the Pentecost storm from 1800 to 2200 UTC 9 Jun 2014. Shown are the reports of severe wind gusts (yellow rectangles) and large hail (green triangles) from the European Severe Weather Database (ESWD; Dotzek et al. 2009). The railroad network is indicated by the white lines and the damaged railroad tracks in NRW are colored red (source: Deutsche Rück 2015). The estimated maximum wind gusts (m s ^{1}) based on in situ measurements are denoted by the dark blue contour lines. The small arrows near the contour line labels indicate the direction of increasing wind speed. The inset on the bottom right hand side shows the location of NRW (shaded in orange) in western Europe.

associated pressure gradients within their convective cells. The necessary ingredients for well-organized MCSs are sufficient amounts of moisture in the boundary layer, latent tropospheric instability [i.e., presence of convective available potential energy (CAPE)], vertical wind shear between the surface and midtroposphere (e.g., Brooks et al. 2003; Brooks 2009), and a lifting mechanism that triggers the convection. In particular, discriminating ingredients for severe-wind-producing convective systems are 1) steep low- to midlevel lapse rates of about 6.5 K km ^{1}, 2) wind shear of at least 15 m s ^{1} between the surface and 6-km altitude, 3) average lower- to midtropospheric wind speeds of at least 10 m s ^{1}, and 4) a parallel orientation between deep-layer wind and shear vectors leading to a fast system propagation (Evans and Doswell 2001; Cohen et al. 2007; Púčik et al. 2015). It is also generally accepted that low-level shear (0 3 km) with a magnitude of at least 10 15 m s ^{1} is needed for long-lived linear MCSs to occur (e.g., Coniglio and Stensrud 2001; Weisman and Rotunno 2004). However, Evans and Doswell (2001) and Cohen et al. (2007) showed that low-level shear is not a discriminating ingredient for severe convective windstorms.

Houze (1993) defined an MCS as a cloud system containing numerous cumulonimbus cells with a contiguous precipitation area of 100 km or more in the horizontal direction. MCSs typically consist of a convective precipitation region and a large region of stratiform rain, including an embedded vertical mesoscale circulation that is often self-sustaining (Houze 2004). The convective line of an MCS can be connected to leading, trailing, or parallel stratiform precipitation (Parker and Johnson 2000). Linear MCSs also exhibit a variety of distinct radar echo patterns, such as a squall line, bow echo structures (Fujita 1978), or line echo wave patterns (Nolen 1959). Fujita (1978) first described the typical life cycle of a bow echo and its dynamical characteristics, such as the rear-inflow jet (RIJ) and the downbursts at the bow's apex. Bow echoes have mainly been studied in the United States, where they are

frequently observed, but they also occur in Europe, featuring similar characteristics to those observed in North America (e.g., Ramis et al. 1997; Schmid et al. 2000; Gatzen 2004, 2013; Punkka et al. 2006). Gatzen (2013) analyzed warm-season convective wind events in Germany, and he found that only eight convective events and two bow echo events resulted in wind speeds above 40 m s^{-1} during the 15-yr period (1997–2011). In addition, mesovortices are known to occur within MCSs, either as 1) midlevel bookend mesovortices (e.g., Weisman 1993; Weisman and Davis 1998) or 2) low-level mesovortices along the leading edge of the storm (e.g., Funk et al. 1999; Atkins et al. 2005; Schenkman and Xue 2016). Cloud systems are thus classified according to the occurrence of these features.

The modeling and forecasting of MCSs is a challenging task for numerical weather prediction (NWP) models, as the initiation of cloud formation and convective processes is frequently not well simulated (e.g., Baldauf et al. 2011). The development of the systems in numerical models is quite sensitive both to the initial and boundary data (Kühnlein et al. 2014), and to the accurate representation of physical and dynamical processes such as boundary layer processes (e.g., convergence), which defines the location where the convective development is triggered (Bennett et al. 2006; Barthlott et al. 2011). The possibility of redevelopment makes the task even more challenging from a modeling perspective, since insufficient initial convective development will lead to a misrepresentation of its further development. In general, the consideration of high-resolution, nonhydrostatic, and thus convection-permitting models leads to better results (e.g., Kain et al. 2006; Weisman et al. 2008; Clark et al. 2009; Warren et al. 2014; Leutwyler et al. 2016).

The purpose of this study is to analyze the synoptic characteristics and the predictability of the Pentecost storm. With this aim, we investigate the presence of the ingredients necessary for the development of severe MCSs. Satellite measurements, weather station observations, as well as numerical weather prediction model data enable a detailed view of this extreme event. Given the poor performance of the operational forecasts, high-resolution hindcast experiments are performed to investigate the reasons for this shortcoming.

A recent study by Barthlott et al. (2017) evaluated the predictability of the event based upon differing domain sizes, microphysical parameterizations, aerosol concentrations, and initialization dates. Our experiments focus on the role of different initial conditions in order to obtain a better simulation of the Pentecost storm of 9 June 2014.

This study is structured as follows. Section 2 describes the data and methods. An overview of the synoptic situation and the preconvective environmental conditions is provided in section 3. The evolution of the convective system is described in section 4, with a major focus on the mechanisms responsible for the severe surface winds. Section 5 analyzes the model experiments and discusses the predictability issues. The last section includes a short summary and our conclusions.

2. Data and methods

The observational data used in this study were obtained from various sources, including two synoptic surface weather station networks, one sounding station, and satellite and operational radar network data. The station network operated by the DWD provides 10-min and hourly weather observations. In particular, data from Düsseldorf Airport (WMO 10400; see Fig. 2) are analyzed. Additionally, data from an automatic weather station network operated by the private weather service MeteoGroup are included. The 1800 UTC sounding from Bergen-Hohne (WMO 10238; see Fig. 2) is considered as representative for the environmental conditions during the passage of the storm. Five-minute volume and precipitation radar scans from Essen (WMO 10410; see Fig. 2), 15-min satellite images from the Meteosat Second Generation (Schmetz et al. 2002), lightning data from the Lightning Detection Network (LINET; Betz et al. 2009), and data from the DWD C-band radar network (Helmert et al. 2014) are used to document the evolution of the MCS. Additionally, operational model data from the European Centre of Medium-Range Weather Forecasts (ECMWF) and from the Consortium for Small-Scale Modeling (COSMO) for medium-resolution [COSMO-EU, 7-km horizontal resolution; Schulz and Schättler (2014)] and high-resolution [COSMO-DE, 2.8-km horizontal resolution; Baldauf et al. (2011)] are considered (Table 1). Precipitation data from the Global Forecast System (GFS) NWP model are also included (Table 1). Satellite, radar, lightning, and operational model data were processed and visualized with the NinJo meteorological workstation system of the DWD (Joe et al. 2005).

To hindcast the storm, the COSMO model (version 5.0) was used in its climate version (CLM), henceforth termed CCLM (Rockel et al. 2008). At high resolutions (grid spacing < 4 km) the model is able to resolve deep convection [convection-permitting model; Prein et al. (2015)], while shallow convection is still parameterized. The CCLM has been successfully applied in several convection-permitting modeling studies in the recent past (e.g., Fosser et al. 2015; Ludwig et al. 2015; Leutwyler et al. 2016).

A three-step one-way nesting approach is applied to the experiments. The horizontal resolution of the parent

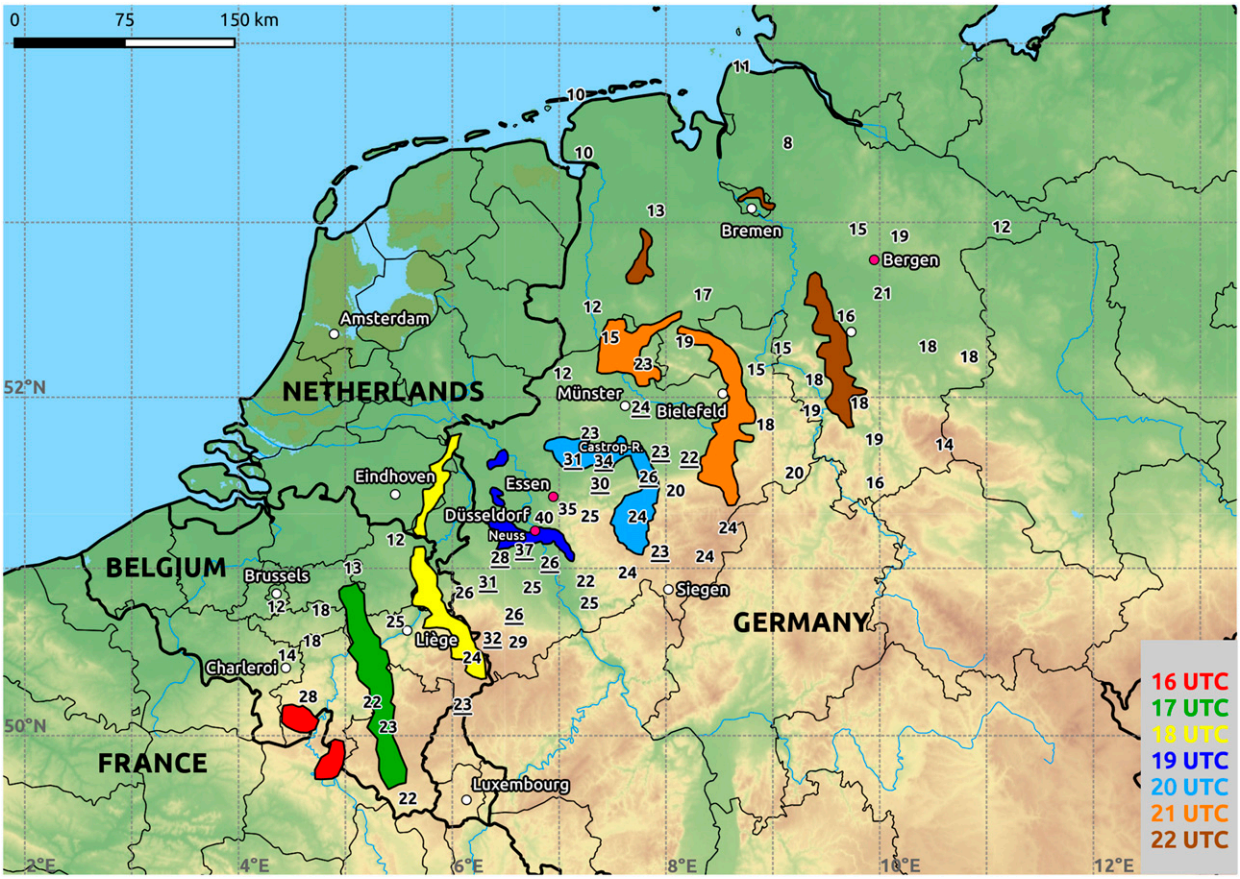

FIG. 2. Illustration of the propagation of the radar echo and observed maximum wind gusts (m s $^{-1}$) of the Pentecost storm on 9 Jun 2014. Radar reflectivity above 40 dBZ at the leading edge of the storm system is shaded in various colors according to the hourly appearance times (see legend). Gust reports from stations operated by the MeteoGroup are underlined. The magenta dots indicate the reference locations (Düsseldorf, Essen, and Bergen Hohne) that are regularly quoted in the text.

domain is 0.22° (D1), the second is 0.0625° (D2), and the final domain reaches a convection-permitting resolution of 0.025° (D3; see Fig. 3 and Table 2). In the first two nesting steps, the convective mass flux is parameterized following the work presented in Tiedtke (1989). For the highest-resolution run, this scheme is applied only to shallow convection without generating subgrid-scale precipitation. An extended description of the physical parameterizations is given in Table 2 and in Doms et al. (2011). All simulations are initialized at 0600 UTC 9 June 2014, approximately 4 h before the initial convection over France and about 10 h before the Pentecost storm was initiated, which reached its peak intensity around 1900 UTC (see section 4). This permits the modeled convective system to form and develop inside the parent model domain.

A set of hindcast simulations is performed with 6-hourly initial and boundary conditions taken both from the ECMWF operative analysis and from the ERA-Interim reanalysis [ERAI; Dee et al. (2011)]. Both are based on the Integrated Forecast System (IFS) model, but correspond to two different model cycles (ERA-Interim, Cy31r2; operative analysis during June 2014, Cy40r1). Thus, they have different spatial resolutions (ERA-Interim T255, approximately 80 km; ECMWF operative analysis T1279, approximately 16 km) and different data assimilations, since the corresponding assimilation cycles use diverse model statistical errors, quality control checks, observation weights, etc. for the calculations, which in the end leads to two distinct datasets (Dee et al. 2011). We investigate the effects of these different initial and boundary conditions on the development of the event and compare the simulated convective event to observations to evaluate the model performance.

To test the sensitivity of the initial conditions to storm development, a sequence of sensitivity studies is designed, where individual variables are substituted into the ECMWF datasets (operative analysis and re-analysis). These sensitivity simulations are forced by

TABLE 1. Specifications of the operational models (GFS, IFS/ECMWF, COSMO EU, and COSMO DE) and the CCLM sensitivity studies.

Simulation	Simulation origin	Initial and boundary conditions	Domain
GFS	NCEP		Global
IFS	ECMWF		Global
COSMO EU	DWD	GME (DWD's operational global NWP model)	DWD Europe
COSMO DE	DWD	COSMO EU	DWD Germany
CCLM ERAI	This study	ERA Interim	D1, D2, D3
CCLM AN	This study	ECMWF analysis	D1, D2, D3
CCLM AN+eraiQV	This study	ECMWF analysis + ERA Interim specific humidity	D1, D2, D3
CCLM AN+eraiU V	This study	ECMWF analysis + ERA Interim wind	D1, D2, D3
CCLM AN+eraiT	This study	ECMWF analysis + ERA Interim temp	D1, D2, D3
CCLM AN+eraiPP	This study	ECMWF analysis + ERA Interim pressure	D1, D2
CCLM AN+eraiQC	This study	ECMWF analysis + ERA Interim cloud liquid water content	D1, D2
CCLM AN+eraiQI	This study	ECMWF analysis + ERA Interim cloud ice content	D1, D2
CCLM AN+eraiT SO	This study	ECMWF analysis + ERA Interim soil temp	D1, D2
CCLM AN+eraiW SO	This study	ECMWF analysis + ERA Interim soil water content	D1, D2

initial conditions from the operative analysis, with one specific initial variable exchanged by the values from ERA-Interim (see Table 1). These specific variables are only changed in the initial time step and for the parent model domain (0.22°). Since both ECMWF datasets represent basically the same synoptic background, the overall changes in the initial data are rather moderate. Still, the initial dataset contains unbalanced information for the mass and wind fields. This will lead to artificial high-frequency oscillations of large amplitude at the start of the simulation and an unwanted extension of the spinup time. Therefore, the data are modified during the initialization process to reduce the unbalanced gravity and sound wave components to a realistic level following a time-filtering approach, as in Lynch (1997): the high frequencies are removed by applying a digital filter to a short time series of the prognostic model variables obtained by an integration from the initial data. Thus, the differences between the exchanged data (and possible physical inconsistencies) are adjusted during the first time steps of the model integration. The specific initial variables considered are the specific humidity QV, temperature T, horizontal wind components U and V, cloud liquid water content QC, cloud ice content QI, deviation from model reference pressure P, soil temperature T SO, and soil water content W SO.

3. Synoptic situation and environmental preconditions

On Pentecost Monday, an upper-level long-wave trough was located above the northeastern Atlantic, while an upper-level ridge extended from Algeria, over northern Italy to Poland (Fig. 4a). Western Europe was therefore located between the upper-level trough and the ridge, which resulted in an upper-level anticyclonically curved southerly to southwesterly flow, such that a weakly forced synoptic regime was in place. Subtropical air masses in the lower troposphere were advected toward central Europe ahead of the trough, resulting in considerable warm-air advection and a hot spell with daily maximum temperatures above 30°C over western Germany. The upper-air trough corresponded with the weak surface low ''Ela,'' located west of Ireland, while the ridge was linked to the surface high ''Wolfgang'' over eastern Europe (Fig. 4). Over western Europe, the pressure field was amorphous because of the very weak pressure gradient. A diffuse and wavy quasi-stationary

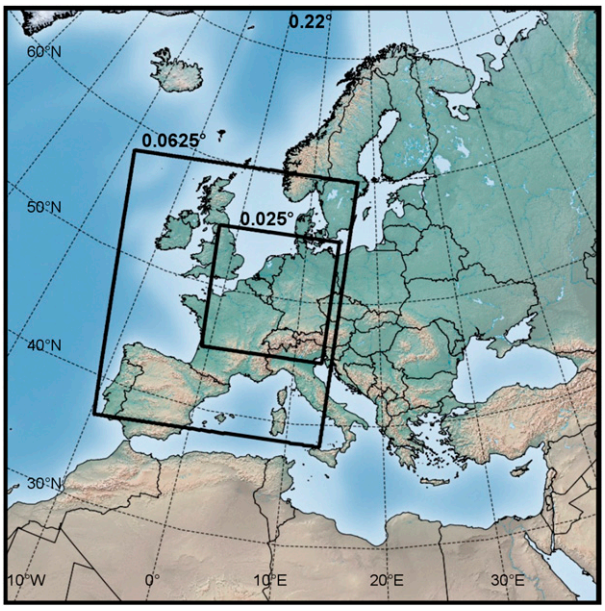

FIG. 3. Model domains used for the three step nesting of the hindcast simulations. The borders of the map indicate the 0.22° parent model domain.

TABLE 2. Specifications of the physical parameterizations used in the different CCLM domains.

Domain	D1	D2	D3
Horizontal resolution (°)	0.22	0.0625	0.025
No. of vertical layers	40	50	50
Convective parameterization	Tiedtke (1989)	Tiedtke (1989)	Only shallow convection after Tiedtke (1989)
Grid scale precipitation	Two category ice scheme (Doms et al. 2011)	Two category ice scheme (Doms et al. 2011)	Three category ice or graupel scheme (Doms et al. 2011)
Radiation	Ritter and Geleyn (1992); Rockel et al. (1991)	Ritter and Geleyn (1992); Rockel et al. (1991)	Ritter and Geleyn (1992); Rockel et al. (1991)
Soil model	Multilayer soil model (TERRA ML) after Jacobsen and Heise (1982)	Multilayer soil model (TERRA ML) after Jacobsen and Heise (1982)	Multilayer soil model (TERRA ML) after Jacobsen and Heise (1982)

front extended from Spain over western France to the North Sea (Fig. 4b).

The large-scale preconditions associated with the storm are examined in detail based on the COSMO-EU and COSMO-DE operational model data and upper-air soundings (Figs. 5 and 6). The ingredients-based forecast of Johns and Doswell (1992) prescribes three elements for the occurrence of deep convection. At first, a sufficient amount of moisture in the boundary layer is required. In this case, enhanced low-level moisture is apparent in the vicinity of the frontal zone, with specific humidity values between 10 and 14 g kg ^{1} over western France, the Benelux region, and northern Germany (Fig. 5a). The 1800 UTC sounding from Bergen-Hohne indicated a comparable mean mixing ratio of 13.1 g kg ^{1} and a mean dewpoint of 17.7°C in the lowest 50-hPa mixed layer (Fig. 6).

The second necessary ingredient is a sufficiently steep lapse rate above the moist layer in the lower to midtroposphere. In this case, conditionally unstable air covered central Europe, with lapse rates of 7 9 K km ^{1} roughly between 800 and 600 hPa (Fig. 5b), which is also documented by the 1800 UTC upper-level observations (Fig. 6). These values are well above the median values, indicating the potential for the occurrence of severe or extremely severe hazardous convective weather (Púčik et al. 2015). The main contributor to these steep lapse rates is the Spanish plume (Morris 1986; van Delden 1998), which features warm and dry air lifted from the Spanish plateau and advected toward western Europe ahead of the upper-air trough. This process is noticeable in the observations at Bergen-Hohne, as indicated by the elevated mixed layer (EML) between 800 and 650 hPa. This is also true for the COSMO-DE vertical profile at Essen (Fig. 6), but slightly modified due to a simulated cloud layer at 750 hPa. The combination of a moist boundary layer and steep midtropospheric lapse rates resulted in moderate-to-high CAPE values of about 2000 3000 J kg ^{1} (Figs. 5a c; Table 3), although the EML capped this energy and led to a significant convective inhibition (CIN; Table 3). This thermodynamic state is also often referred to the so-called loaded-gun scenario (Fawbush and Miller 1952).

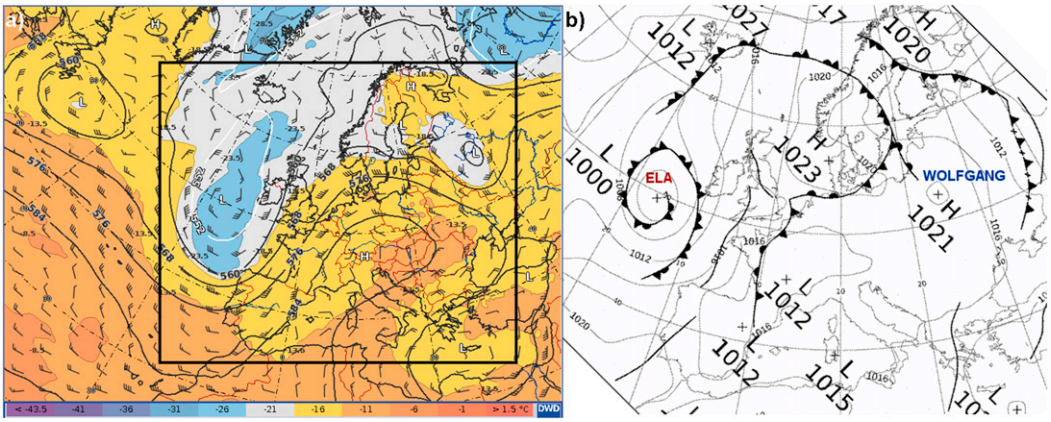

FIG. 4. (a) Analysis of geopotential height (gpdm; black lines), wind speed (kt, where 1 kt 0.51 m s ^{1}; wind barbs), and temperature (°C; colored) at the 500 hPa pressure level and (b) surface weather chart of mean sea level pressure (hPa) and fronts at 1200 UTC 9 Jun 2014 (source: Met Office). The black rectangle in (a) denotes the area shown in (b).

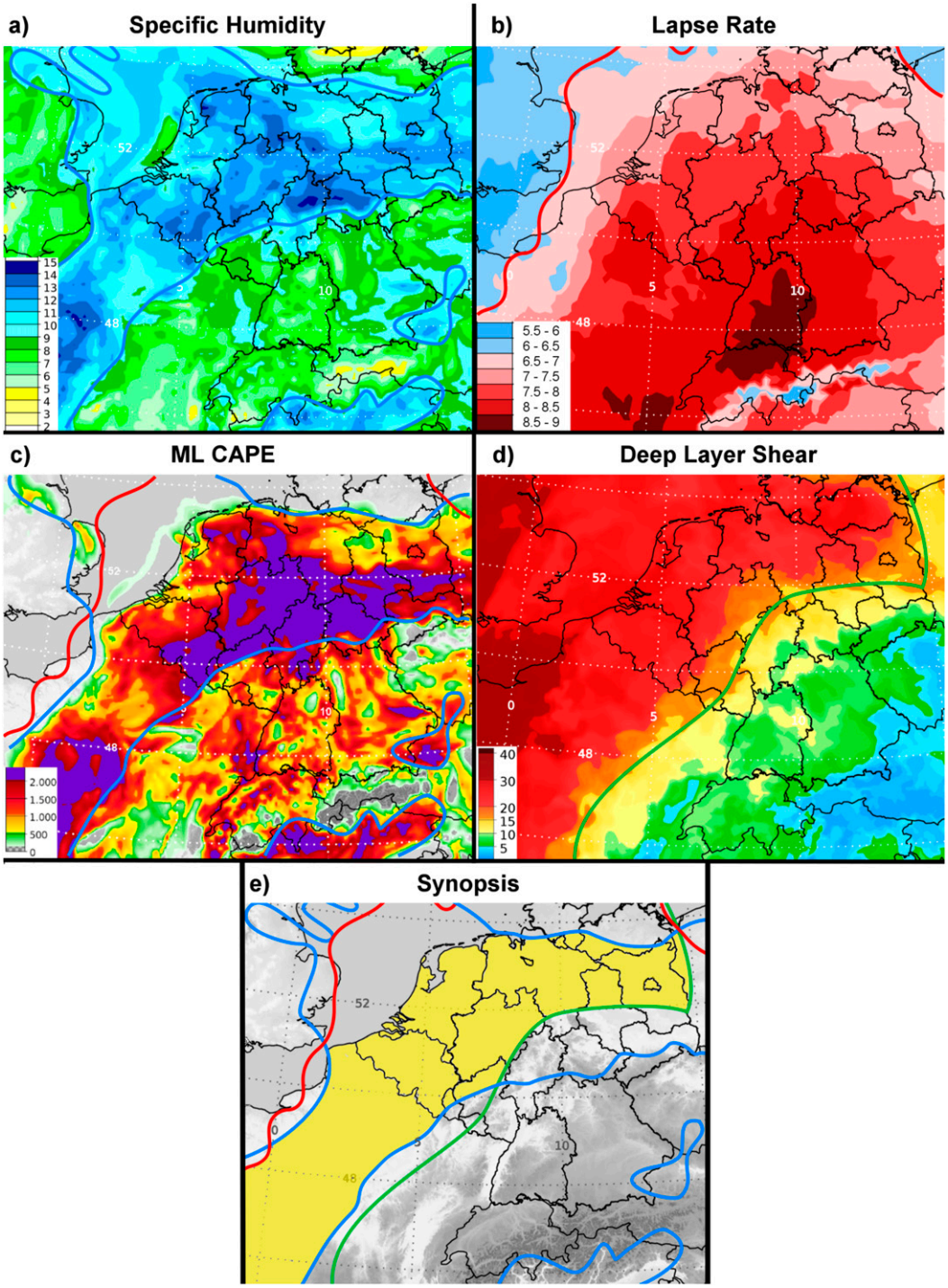

FIG. 5. Forecast at 1800 UTC 9 Jun 2014 of the 1200 UTC COSMO EU run in terms of (a) specific humidity (g kg ^{1}) at a height of 200 m, (b) the 800 600 hPa lapse rate (K km ^{1}), (c) the 50 hPa mixed layer (ML) CAPE (J kg ^{1}) and thresholds of (a) and (b), (d) the deep layer shear (in m s ^{1}), and (e) the overlap of thresholds for (a), (b), and (d) marked in yellow. Shown are thresholds for the thick colored lines: specific humidity in (a), 10 g kg ^{1}; 800 600 hPa lapse rate in (b), 6.5 K km ^{1} (Púčik et al. 2015); and deep layer shear in (d), 15 m s ^{1} (Púčik et al. 2015). The area shown corresponds to the inner domain (D3) in Fig. 3.

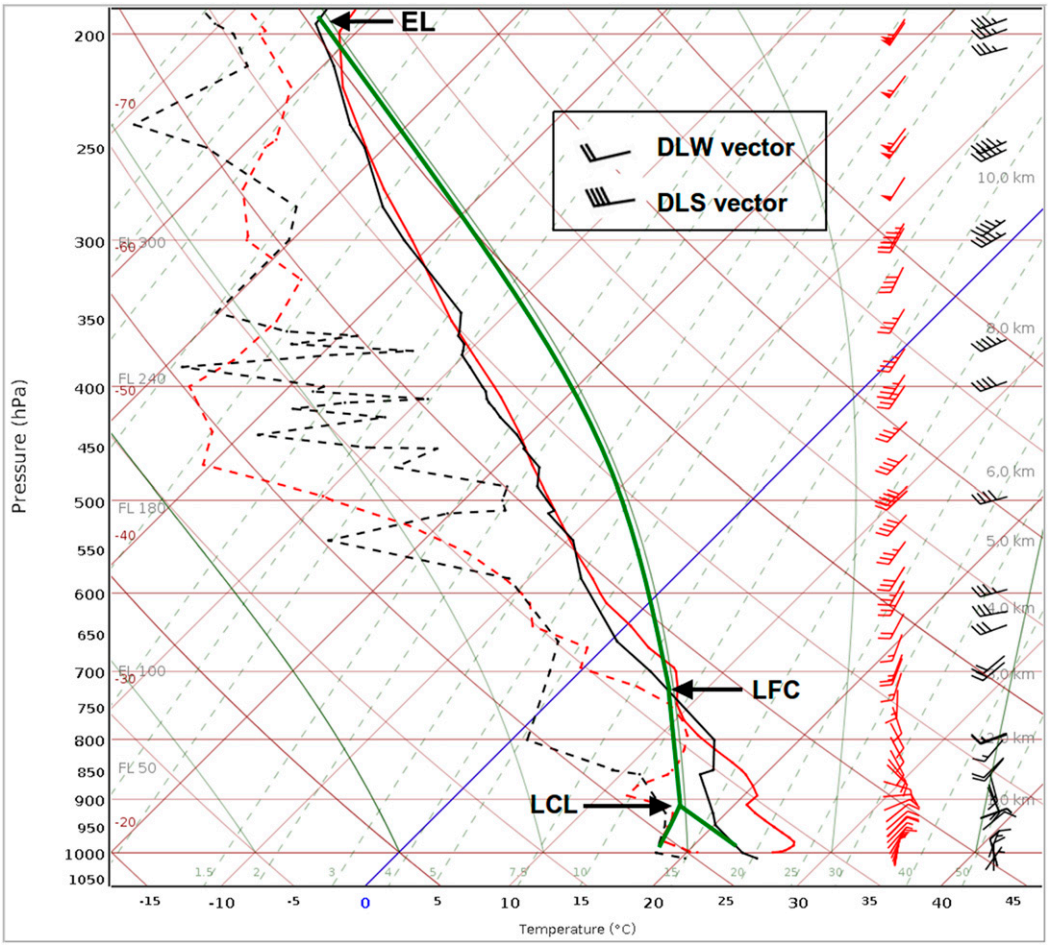

FIG. 6. Skew T log$p$ diagram of upper air observations from Bergen Hohne (WMO 10238; 52°48′N, 9°55′E; black lines) and of the COSMO DE analysis sounding from Essen (51°27′N, 7°0′E; red lines) at 1800 UTC 9 Jun 2014. The solid (dashed) thick lines represent temperature (dewpoint) values. The ascending trajectory of a 50 hPa thick ML parcel for the observational sounding from Bergen Hohne is shown by the green line with its lifted condensation level (LCL), level of free convection (LFC), and equilibrium level (EL). The DLS and deep layer wind (DLW) vectors calculated from the Bergen Hohne sounding are also shown.

Finally, vertical wind shear is an additional crucial ingredient for well-organized MCSs, as shown in various numerical and observational studies (e.g., Weisman and Klemp 1982; Rasmussen and Blanchard 1998). The wind shear between 0 and 6 km is the so-called deep-layer shear (DLS). In this case, the DLS reached values of 15 25 m s ^{1} over large parts of France, Benelux, and northwestern Germany (Fig. 5d). The sounding observation from Bergen-Hohne revealed a DLS vector with a magnitude of 21 m s ^{1} at 252° (WSW) and the 0 6-km mean wind (deep-layer wind) vector had a magnitude of 11 m s ^{1} at 250° (Fig. 6). Thus, both vectors were nearly parallel and were of sufficient strength, which favored a fast downwind-propagating and severe MCS (Corfidi 2003; Cohen et al. 2007). Moreover, the observational sounding indicated low-level shear (0 3 km) of about 12 m s ^{1}, which is in the range of the values found by Evans and Doswell (2001) and Cohen et al. (2007). This value is slightly weaker compared with the 0 2.5-km shear values used in the idealized simulation of a well-organized bow echo by Weisman and Rotunno (2004). The last indispensable ingredient, the lifting mechanism, was provided by the outflow from a decaying multicellular convection system above northern France (for more details see section 4).

In brief, the synoptic situation created favorable environmental conditions for the development of organized MCSs, and the four necessary ingredients for severe wind events are in place (see introduction). Therefore, severe weather was highly probable over large parts of western Europe on the late afternoon of 9 June 2014 (yellow area in Fig. 5e). The environmental

TABLE 3. Values of CAPE, CIN, and DLS calculated for the two vertical profiles shown in Fig. 6.

Parameter	Observational sounding, Bergen (1800 UTC)	COSMO DE analysis vertical profile, Essen (1800 UTC)
50 hPa mixed layer CAPE (J kg ^{1})[a]	1799	2583
50 hPa mixed layer CIN (J kg ^{1})[a]	−85	−70
Most unstable CAPE (J kg ^{1})[a]	3026	3171
Most unstable CIN (J kg ^{1})[a]	−1	−90
DLS (m s ^{1})	21.1	21.6

[a] Thermodynamic parameter calculated using the virtual temperature.

conditions were characterized by high boundary layer moisture, steep midtropospheric lapse rates, and strong vertical wind shear in the lower and middle troposphere. This regime of high CAPE/high DLS (Figs. 5c e and Table 3) generally allows the formation of long-lived MCSs (Coniglio et al. 2010). In particular, a fast and potentially severe MCS was promoted as a result of the relatively strong mid- to upper-tropospheric flow and the alignment of the mean wind and shear vectors (Evans and Doswell 2001; Cohen et al. 2007). However, a capping inversion induced by the Spanish plume had to be overcome to initiate deep convection.

4. Evolution and structure of the bow echo

On 9 June 2014, scattered deep convective cells developed over southwestern France between 0930 and 1130 UTC in the vicinity of the quasi-stationary frontal boundary (Fig. 4b) and then merged into an unorganized multicell cluster. Given its location ahead of the upper-level trough, this cloud system moved northeastward and developed an isolated supercell producing large hail to the east of Paris (not shown). As the decaying cluster reached Belgium at 1600 UTC and became outflow dominant, its outflow boundary interacted with northeasterly surface winds, leading to low-level convergence (feature 1 in Fig. 7b). The forced lifting was able to overcome the CIN. Consequently, several convective cells rapidly developed over southeastern Belgium and remained initially unorganized (Fig. 7c).

Around 1700 UTC, the storm cells strengthened (strong increase of lightning activity) and became linearly organized (Figs. 7d f). The linear convective system was now moving northeastward toward the German Belgian border. The rapid development of the MCS over Belgium was also observable in the satellite imagery. A nearly circular-shaped cloud cluster formed during the period of convective organization between 1600 and 1700 UTC, with a cold-ring feature and a central warm spot (CWS) (feature 3 in Fig. 7d), as shown by the enhanced infrared satellite images (Figs. 7a,d). Recent studies showed that these cloud-top patterns are linked to severe weather conditions (e.g., Irsic Zibert et al. 2010; Setvàk et al. 2010). The convective cloud expanded further until 1800 UTC, retaining its near-circular shape (Figs. 8a,b). In addition, an overshooting top (OT) was visible east of the CWS at 1800 UTC (feature 4 in Fig. 8a) aligned above the strongest radar reflectivity near the German Belgian border (cf. Figs. 8a and 8c). The occurrence of OTs is often related to severe weather phenomena (Bedka 2011; Mikuš and Strelec Mahović 2013). At 1800 UTC, bands of weak radar reflectivity appeared behind the MCS (feature 2 in Fig. 8c). This feature consists of multiple rear-inflow notches (RINs), which often indicate the location of midlevel RIJs (Przybylinski 1995). The RIJ developed and strengthened over eastern Belgium between 1730 and 1800 UTC, reaching velocities of 22 26 m s ^{1} at about 2-km altitude (not shown). At that time, a slight bowing of the convective line can be identified in reflectivity scans (Fig. 8c).

At 1800 UTC, the leading anvil of the linear MCS already covered the western part of NRW, where surface winds were weak with a northerly to northeasterly direction, such that the convergence at the leading edge of the convective line remained (Figs. 8a c). As the RIJ got stronger (>31.5 m s ^{1} at 2-km altitude) and the mesoscale storm moved farther northeast, it evolved into a mature bow echo and reached the Rhine Ruhr metropolitan region around 1900 UTC (Fig. 8f). Likewise, the abundant lightning observations showed a clear bow structure (feature 5 in Fig. 8e). Also noteworthy was the very cold OT (73.5°C) over Düsseldorf (feature 4 in Fig. 8d), indicating that the cloud top penetrated about 1 km into the stratosphere (tropopause was located at about 200 hPa; see Fig. 6) as a result of the extreme updrafts within the bow echo.

Furthermore, the vertical structure of the Pentecost storm is analyzed explicitly. The reflectivity cross section taken through the core and apex of the bow revealed a strong low-level reflectivity gradient, upright convective cells, and a weak-echo region [WER; often named echo overhang; Chisholm (1973)] at the leading edge (Fig. 9a), with the 45-dBZ core extending to a height of approximately 12 km (not shown) and a weaker trailing stratiform region. A WER is an indicator for the location of a strong storm-relative inflow and updraft zone

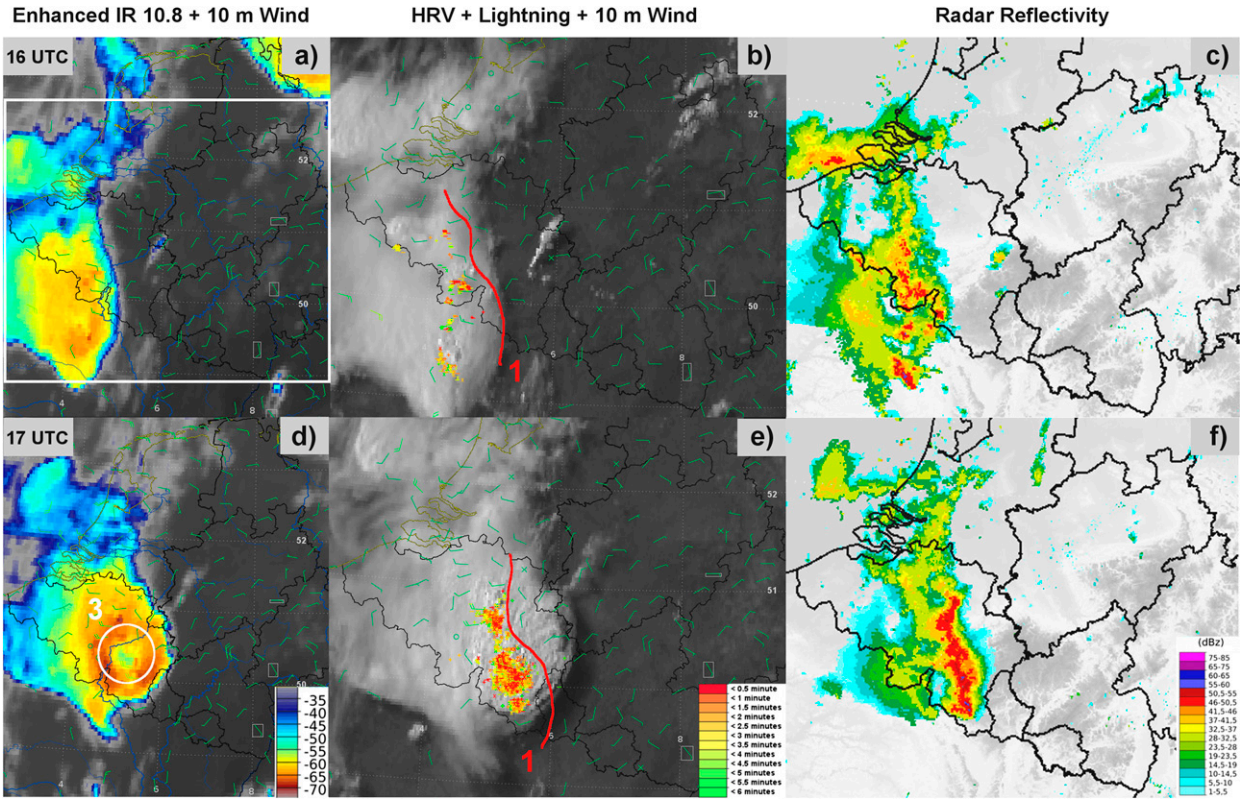

FIG. 7. Evolution of the cloud system of the Pentecost storm above Benelux and NRW between (top) 1600 and (bottom) 1700 UTC 9 Jun 2014: (a),(d) Meteosat 10.8 μm IR channel images with cloud top temperatures (°C) and 10 m wind barbs; (b),(e) Meteosat high resolution visible (HRV) channel images, 10 m wind barbs, and last 6 min lightning flashes; and (c),(f) low level radar reflectivity (dBZ). Features 1 and 3 are discussed in the text. The white rectangle in (a) indicates the domain shown in (b), (c), (e), and (f).

(Lemon 1980). The RIJ is evident by means of the striking RIN area that extends more than 45 km (up to 6 km) toward the low-level reflectivity core of the bow echo (Fig. 9a). Thus, the RIJ probably affected the downdrafts of the storm through a horizontal momentum transfer as well as via evaporative cooling by entrainment of air with low pseudo potential temperatures. In a cross section of the radial velocity taken farther northwest of the apex at 1905 UTC, an RIJ at midlevels (2 6 km) with inbound velocities larger than 31.5 m s ^{1} (indicated by aliasing; see Figs. 9b,c) is detected. It gradually descended to the surface while approaching the leading edge of the system (Fig. 9c). For the southern part of the bow echo, the RIJ remained elevated and did not reach the surface (Fig. 9b).

The link between descending RIJs and straight-line wind damage swaths has been studied in numerous studies using Doppler radar (e.g., Schmidt and Cotton 1989; Burgess and Smull 1990; Atkins et al. 2004). Concurrent with the arrival of the RIJ at the surface, the strongest wind gust of 39.5 m s ^{1} (142.2 km h ^{1}) was measured at Düsseldorf Airport between 1900 and 1910 UTC (cf. Figs. 9c and 11). This value compares reasonably well to the strength of the RIJ and is also comparable to the hurricane-force winds recorded during winter storm Kyrill in 2007 (Fink et al. 2009). Note that the strongest gusts occurred along a small strip (width of about 15 30 km; see Fig. 1) within the Rhine Ruhr region between 1900 and 2000 UTC (e.g., 37 m s ^{1} in Neuss at 1900 UTC, 35 m s ^{1} in Essen at 1930 UTC, and 34 m s ^{1} in Castrop-Rauxel at 1950 UTC; see Fig. 2).

Several studies have shown the importance of (cyclonic or anticyclonic) mesovortices along the bow echo gust front or at the northern part of the bow echo for the production of straight-line surface wind damage (e.g., Trapp and Weisman 2003; Weisman and Trapp 2003; Atkins et al. 2005; Wakimoto et al. 2006a,b; Wheatley et al. 2006). For the Pentecost storm, the mesocyclone detection algorithm (MDA; Hengstebeck et al. 2011; Hengstebeck et al. 2014) of the DWD identified an intense system-scale mesocyclone north of the bow echo apex at 1900 UTC (Fig. 10). This detection is linked to a circulation clearly visible in radial velocities at different radar elevation surfaces (e.g., at the 12°-elevation surface; see feature 1 in Fig. 10a). Yet, this circulation did not reveal the typical dipole structure of a mesocyclone

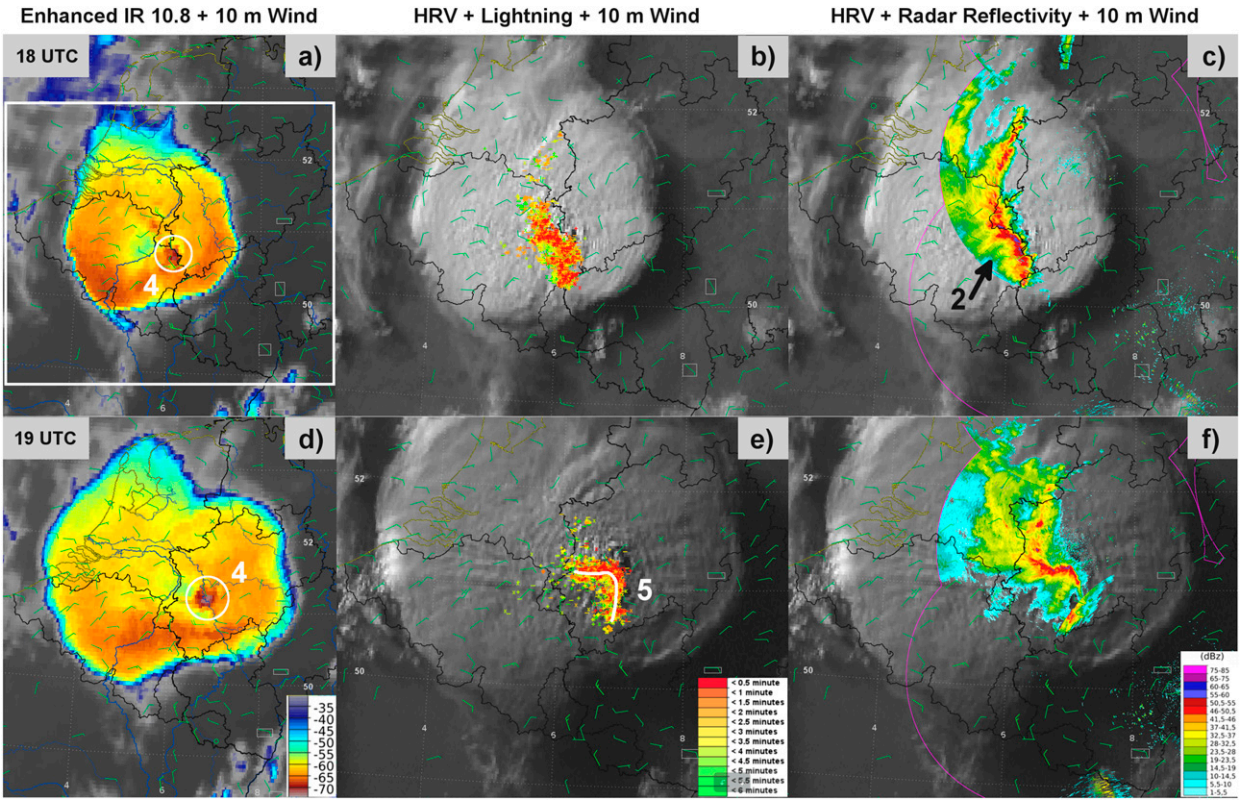

FIG. 8. Evolution of the cloud system of the Pentecost storm above Benelux and NRW between (top) 1800 and (bottom) 1900 UTC 9 Jun 2014: (a),(d) Meteosat 10.8 μm IR channel images with cloud top temperatures (°C) and 10 m wind barbs; (b),(d) Meteosat HRV channel images, 10 m wind barbs, and last 6 min lightning flashes; and (c),(f) Meteosat HRV channel images, 10 m wind barbs, and 0.8° radar reflectivity (dBZ). Features 2, 4, and 5 are discussed in the text. The white rectangle in (a) indicates the domain shown in (b), (c), (e), and (f).

(Brown and Wood 2007). The inbound velocities, corresponding to the RIJ, were much stronger and covered a larger area than the outbound velocities. We hypothesize that a cyclonic bookend vortex formed across the northern part of the bow echo during the bowing stage (1800 1830 UTC) and subsequently amplified the northern part of the RIJ (Weisman 1993). According to Weisman and Davis (1998), bookend vortices result from upward or downward tilting in vertically sheared environments. In our case, the strength of the southerly to southwesterly flow increased with height at midlevels (see Fig. 6), suggesting that downward tilting caused the formation of the northern bookend vortex corresponding to Fig. 5b in Weisman and Davis (1998).

Figure 10 shows the line-end vortex when it reached a maximum shear of 33 m s ^{1} km ^{1} at 1905 UTC (Wapler et al. 2016). The further development of the cyclonic vortex remains unclear because of strong attenuation by hydrometeors, resulting in qualitatively poor scans by the Essen radar station until 2000 UTC. A vertical cross section through the circulation marked in Fig. 10a depicts a mesovortex depth of about 10 km at 1900 UTC (feature 2 in Fig. 10b). Furthermore, the deep meso-β vortex was located near the striking OT (cf. Figs. 10a and 10d) and corresponded well to the reported severe wind gusts (Fig. 1; Wapler et al. 2016, their Fig. 10). These facts suggest that the formation of the bookend vortex strengthened the northern part of the RIJ, which locally descended to the surface and caused the straight-line wind damage swath of the Pentecost storm in the Rhine Ruhr area (Fig. 1).

The observations from the Düsseldorf Airport characterize the impact of the Pentecost storm at the surface (Fig. 11). A peak gust speed of 39.5 m s ^{1} was measured at Düsseldorf Airport between 1900 and 1910 UTC and was accompanied by a wind shift from the northerly to the southwesterly direction. The maximum wind speeds remained above 20 m s ^{1} until 1930 UTC, likely as a result of the presence of convective cells (see rainfall observations in Fig. 11). However, wind gusts remained at about 15 m s ^{1} until 2030 UTC, which might be related to pressure gradients and the vertical advection of momentum from the RIJ. During the next few hours, the

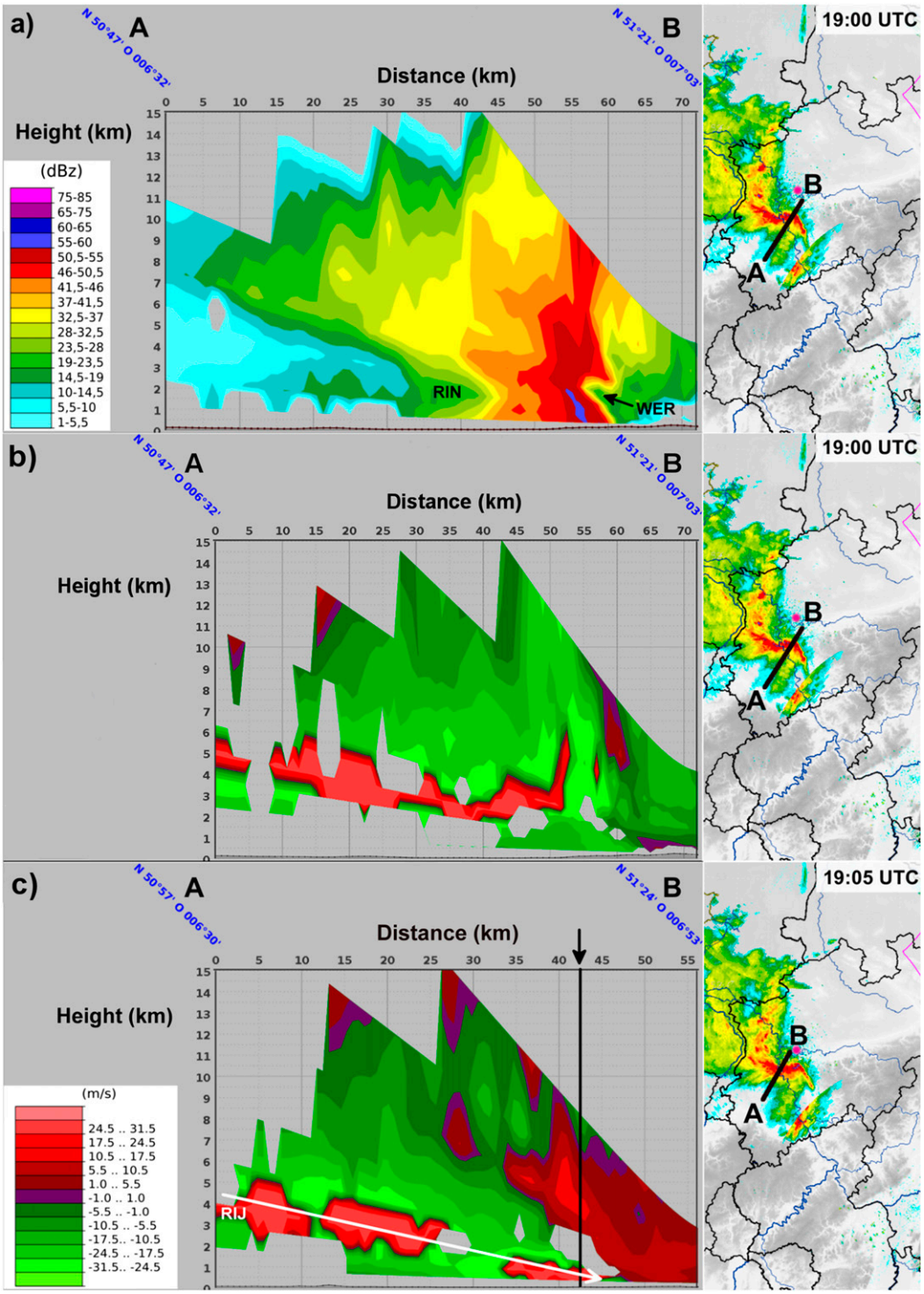

FIG. 9. Vertical cross sections of (a) reflectivity (dBZ) and (b),(c) radial velocity (m s $^{-1}$; red, away from radar; green, toward radar) measured by the Essen radar station (indicated by the magenta dot in the insets) at 1900 UTC in (a) and (b) and at 1905 UTC in (c) 9 Jun 2014. The RIN and the WER are indicated in (a). The black arrow in (c) marks the location of the Düsseldorf Airport and the white arrow in (c) denotes the descending RIJ. Note the aliased radial velocities along the axis of the RIJ in (b) and (c). The insets on the right hand side reveal the cross section paths and 0.8° radar reflectivity.

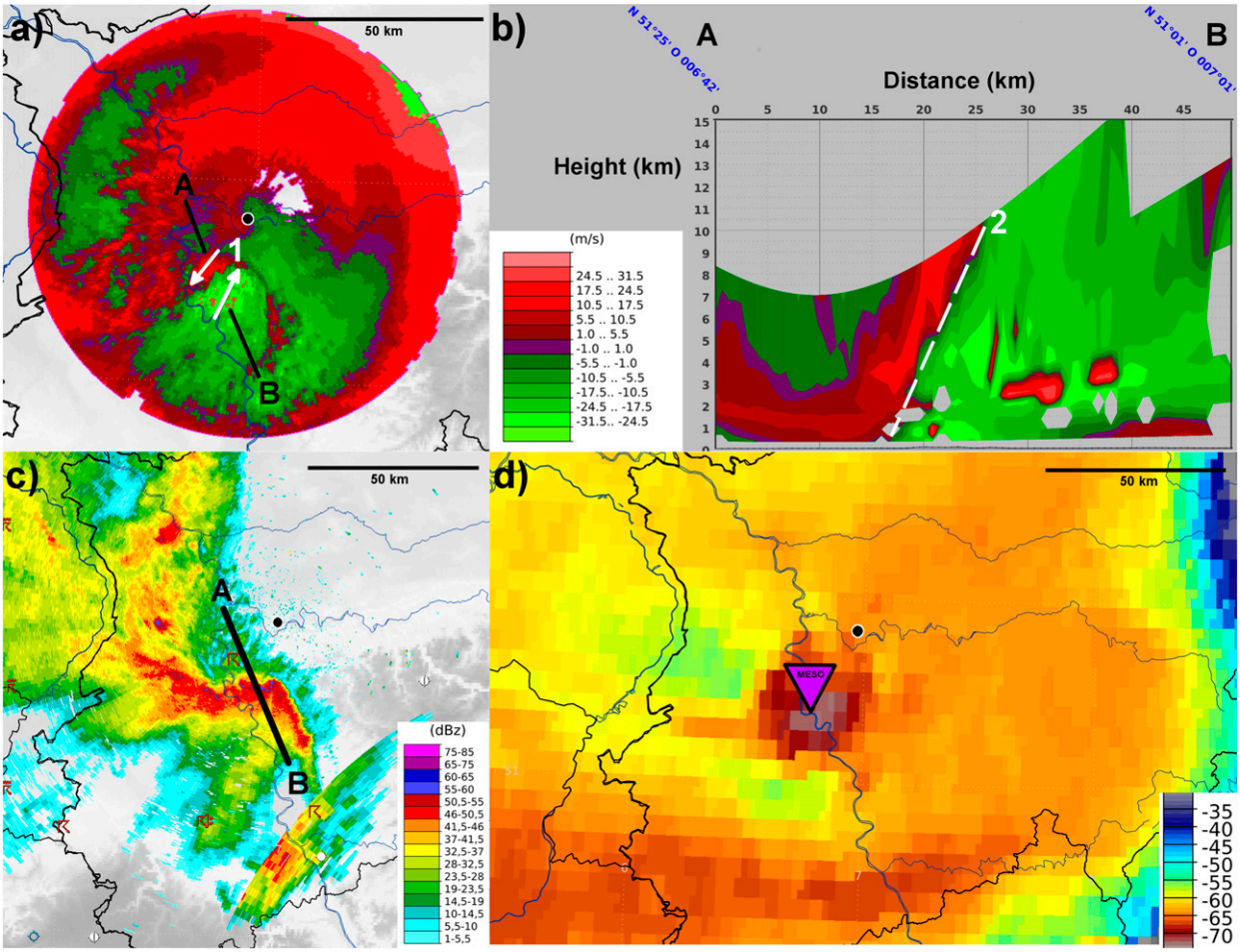

FIG. 10. Detection of the mesocyclone of the Pentecost storm at 1900 UTC 9 Jun 2014: (a) 12° sweep of radial velocity (m s ^{1}) by the Essen radar station. The two white arrows mark the cyclonic mesovortex at a height of about 4 km. (b) Vertical cross section of radial velocity, within the cross section path (A B) shown in (a) and (c). (c) The 0.8° radar reflectivity (dBZ). (d) Meteosat 10.8 μm IR channel image with cloud top temperatures (°C); the solid violet triangle denotes the mesocyclone detected by the DWD MDA. The white edged black dots in (a), (c), and (d) mark the location of the Essen radar station. Features 1 and 2 are discussed in the text.

wind progressively weakened, while the storm moved farther northeast. The surface pressure increased at Düsseldorf by about 5 hPa within 20 min, followed by a slower decrease. This indicates the presence of a meso-high induced by a strong cold pool (cf. also temperature and dewpoint temperature drops of about 10° and 4°C, respectively), which is a typical signature of linearly organized MCSs (Johnson and Hamilton 1988). The pressure drop at 1720 UTC might be associated with a propagating gravity wave (e.g., Bryan and Parker 2010; Adams-Selin and Johnson 2013), probably triggered by the formation of the linear MCS in Belgium. The leading edge of the Pentecost storm caused overall moderate precipitation amounts. Rainfall started at about 1910 UTC after the maximum wind gust, and a peak amount of 12 mm fell between 1910 and 1920 UTC. Altogether, 21 mm of rainfall was measured between 1910 and 1950 UTC at Düsseldorf Airport. The observed altocumulus clouds (Fig. 11) comply with the aforementioned unstable middle troposphere (Fig. 5b).

The Pentecost storm began to weaken over the eastern part of NRW between 2015 and 2045 UTC, as the lightning activity and radar reflectivity slowly decreased (not shown). The bow echo evolved into a comma-shaped and asymmetric system (Fujita 1978) during this period in response to the strengthening of the cyclonic bookend vortex [see the reflectivity structure between 1900 and 2100 UTC in Fig. 2; Skamarock et al. (1994); Weisman and Davis (1998)] and the OT disappeared, which implied a significant weakening of the updraft. The decreasing strength of the wind gusts in eastern NRW (see Fig. 2) can be explained by a less unstable environment near the surface, as the storm probably became more elevated. The dissipating MCS reached

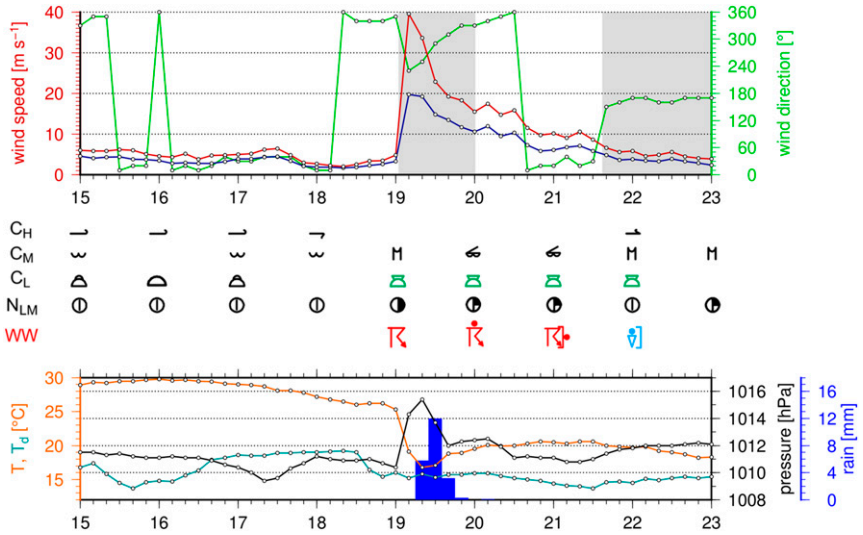

FIG. 11. Surface observations from the Düsseldorf synoptic station (WMO 10400; 51°17′N, 6°47′E) for the period 1500 2300 UTC 9 Jun 2014. (top) Maximum wind gusts (red line) and mean wind speed (blue line) during the preceding 10 min (m s ^{1}), and corresponding mean wind direction (°; green line; southerly and westerly wind directions are shaded gray). (middle) Type of high clouds (C_H), medium clouds (C_M), and low clouds (C_L); cloud cover of C_L and C_M (N_{LM}); and present weather (WW). (bottom) Temperature (°C; orange line), dewpoint tem perature (°C; blue line), surface pressure (hPa; black line), and precipitation amounts (mm; blue bar). Symbols for cloud types, cloud cover, and present weather are typically used in surface charts to plot the information included in surface synoptic observation (SYNOP) reports.

northern Germany at 2230 UTC and gradually lost its organization. A schematic tracking and overview of the progression of the storm is provided in Fig. 2.

5. Predictability and modeling

The Pentecost storm posed considerable problems for operational NWP models, as the strong convective activity over western Germany was not well forecasted, despite the overlap of the necessary ingredients of humidity, instability, and wind shear in the models (Fig. 5). Most NWP models predicted precipitation over northern France, Belgium, and the Netherlands, which is related to the quasi-stationary front west of the area where the storm actually occurred (cf. Figs. 12a e with Fig. 12f). The 1200 UTC operational forecasts from ECMWF and COSMO-DE predicted some precipitation over NRW, but the strongest convective precipitation was still projected to occur over Belgium and the Netherlands (Figs. 12b,d). However, the ECMWF forecast indicates a feature with strong precipitation over northern France, Belgium, and the Netherlands that deviates from the ordinary frontal precipitation regime, thus pointing out the potential for severe weather developments. These forecasts were distributed to operational forecasters at a time (between 1700 and 1800 UTC) when the MCS had already developed. The storm was first well captured by COSMO-DE when the storms' radar observations were assimilated into the initial fields at 1800 UTC, in other words after it was initialized inside the domain (Fig. 12e). The COSMO-DE 1800 UTC forecast was issued between 1900 and 2000 UTC, when the storm already produced severe winds in western NRW (see Fig. 2). In summary, the operational forecasts did not capture the development well. Nevertheless, it is also evident that the COSMO model is able to simulate a bow echo, given the correct initial and boundary conditions (COSMO-DE 1800 UTC run).

Model hindcast experiments are used to complement the description of the extreme convective event. We found that the event can be better reproduced with CCLM using ERA-Interim for the initial conditions at 0600 UTC than with initial conditions derived from the operative ECMWF analysis. The ERA-Interim-driven CCLM simulation (CCLM ERAI; see Table 1) is considerably closer to reality than the operational forecasts (Fig. 12) in terms of the observed features and the spatiotemporal evolution of the Pentecost storm, even though it is slightly shifted to the northwest (Figs. 13 and 14). CCLM ERAI features a mature MCS with a bow echo signature that appeared over the southern

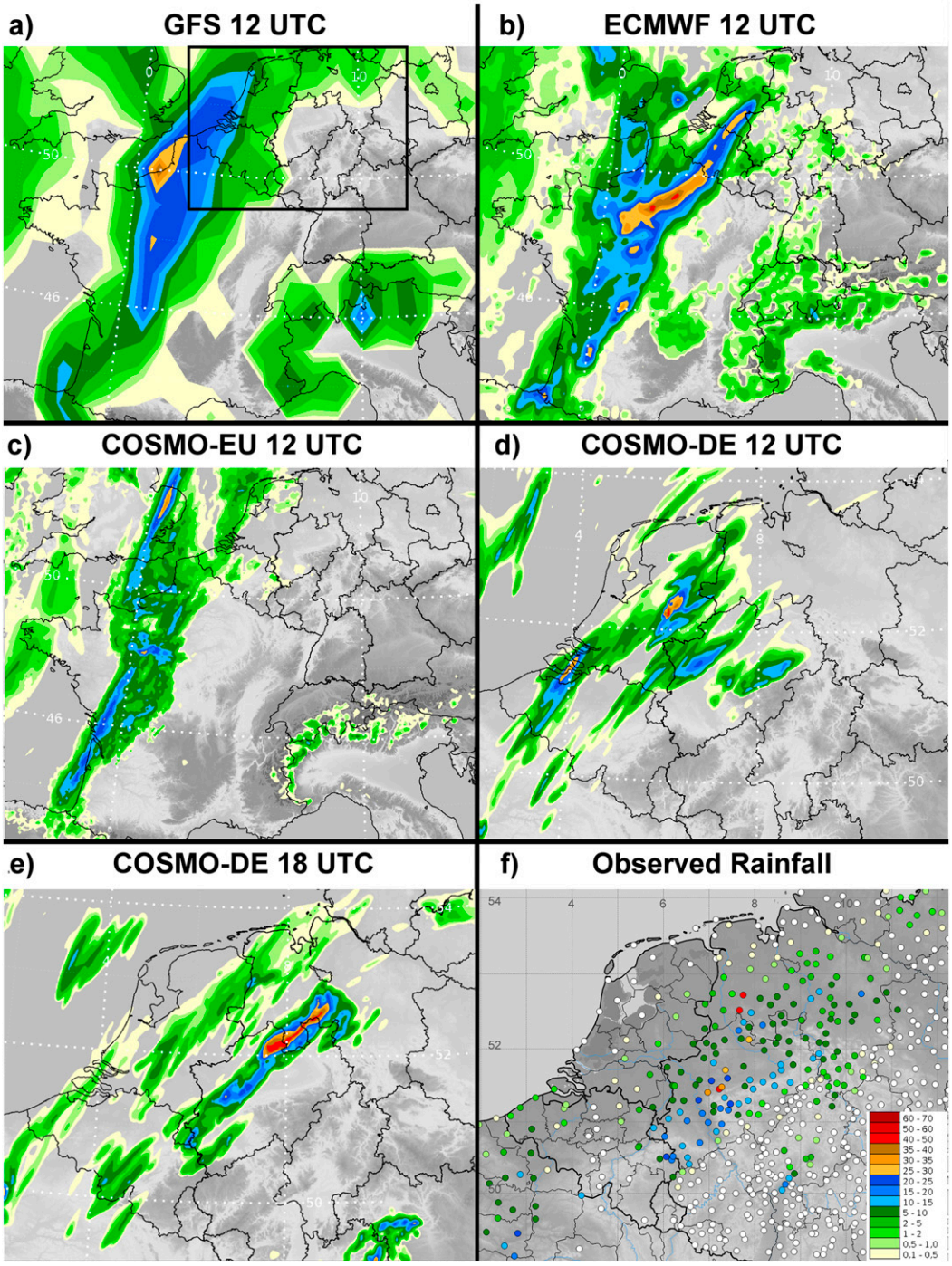

FIG. 12. The 12 h precipitation accumulation (1200 UTC 9 Jun 0000 UTC 10 Jun 2014) forecasted by the 1200 UTC runs of (a) GFS, (b) ECMWF, (c) COSMO EU, and (d) COSMO DE. (e) The 6 h precipitation accumulation (1800 UTC 9 Jun 0000 UTC 10 Jun 2014) forecasted by the 1800 UTC run of COSMO DE and (f) observed by synoptic stations. The black rectangle in (a) indicates the area shown in (d), (e), and (f).

Netherlands at 1800 UTC (Fig. 14a), which formed by the merging of single cells initiated over northern France. These initial cells in our CCLM ERAI simulation were induced by the cold outflow of previous convection over northwestern France, which is similar to the observed triggering process (see section 4). The simulated bow echo moved northeastward and reached western NRW at 1900 UTC, with an active bookend

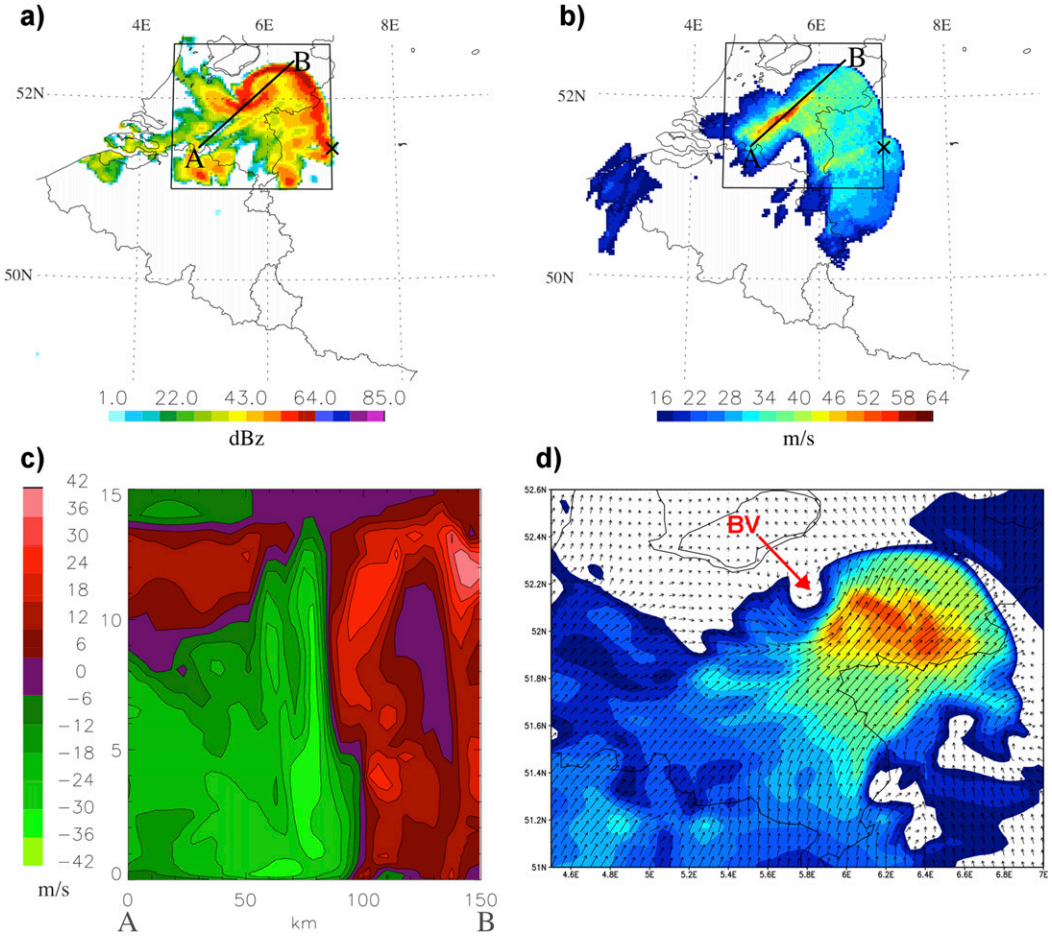

FIG. 13. Results from CCLM ERAI at 1900 UTC. (a) Radar reflectivity at approximately 1.3 km altitude (dBZ), (b) 10 m maximum wind (m s $^{-1}$), (c) cross section of the radial wind component (m s $^{-1}$) with respect to the Essen radar station [denoted by a cross in (a) and (b)], and (d) wind speed (shading; m s $^{-1}$) and direction (arrows) at approximately 2.8 km altitude, in the rectangle denoted in (a) and (b). The northern bookend vortex (BV) is indicated in (d). The domain shown in (a) and (b) corresponds to the area shown in Figs. 7c,f and 8c,f.

vortex in the northern part of the bow echo (Figs. 13c,d). The vertical cross section through this cyclonic circulation shows that the mesovortex extends through the whole troposphere (Fig. 13c), which is comparable to the real case (cf. Figs. 10b and 13c).

The peak intensity of the system as related to convective wind gusts was simulated between 1900 and 2000 UTC along the path of the bookend vortex (Fig. 13b). However, CCLM ERAI overestimated the maximum wind compared with the observations (58 vs 40 m s $^{-1}$). Furthermore, the horizontal cross section of the horizontal wind field featured a midlevel RIJ behind the leading edge of the storm (Fig. 13d). Likewise, a strong low-level radar reflectivity gradient at the leading edge of the MCS was present in the simulation (Fig. 13a). Thus, we conclude that the modeled convective system has similar characteristics to those observed in the real convective storm (e.g., bow echo, RIJ, bookend vortex; see section 4).

To study the potential predictability of the event, CCLM hindcasts were also performed with the ECMWF operational analysis as the initial and boundary conditions (Table 1). These simulations were started at the same time (0600 UTC) as for the ERA-Interim-driven simulation. The ECMWF operative analysis driven simulation (CCLM AN; see Table 1) also developed a convective storm, but its track is clearly displaced to the west (Fig. 14b), similar to the operational forecasts. Moreover, the bow echo structure of the simulated storm was less pronounced compared to the ERA-Interim-driven simulation (cf. Figs. 14a and 14b). Thus, the reanalysis provides better initial fields for the generation of the storm in spite of its lower resolution compared to the analysis. The comparison of the two

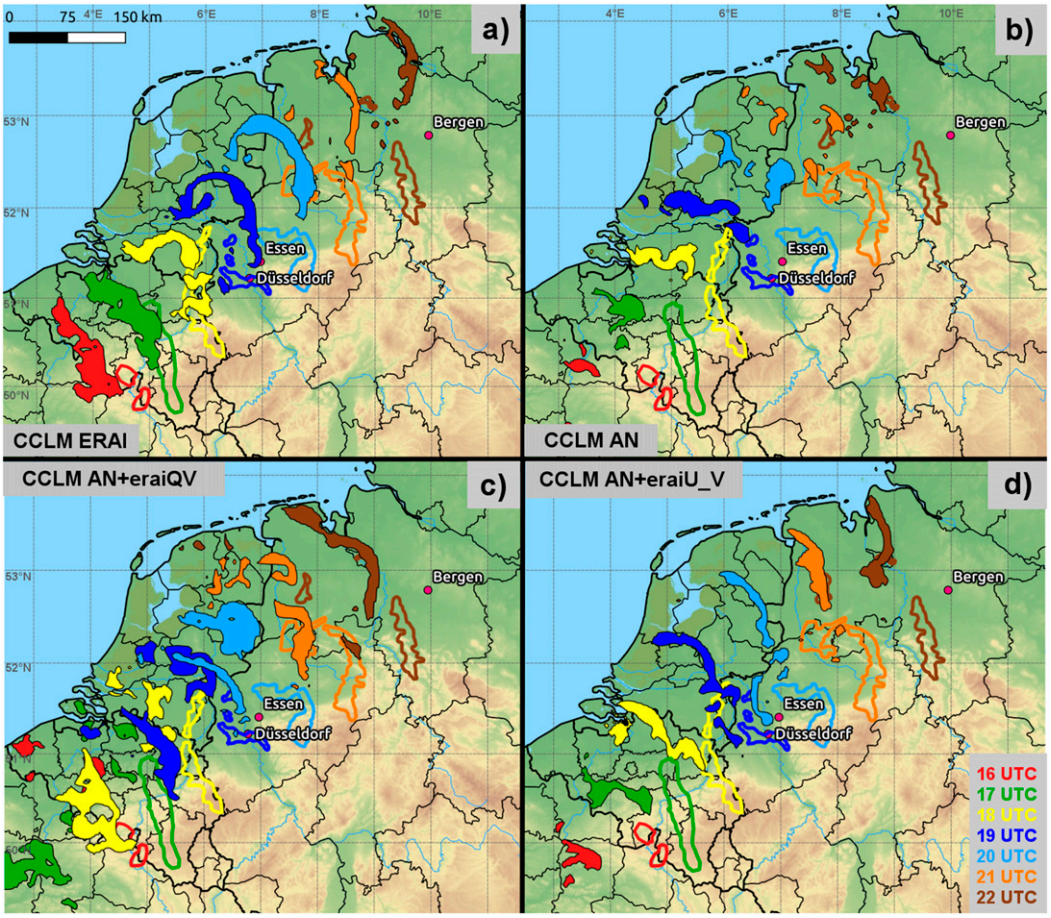

FIG. 14. Simulated radar reflectivity (shaded) over the 50 dBZ threshold at approximately 1.3 km altitude and observed 0.8° radar reflectivity (colored isolines) over the 40 dBZ threshold in consecutive time steps (see legend; 1600 2200 UTC 9 Jun 2014) in the (a) CCLM ERAI, (b) CCLM AN, (c) sensitivity CCLM simulation with altered initial specific humidity (CCLM AN+eraiQV), and (d) sensitivity CCLM simulation with altered initial horizontal wind (CCLM AN+eraiU V; see details in section 2 and Table 1). Note that the simulated and observed re flectivities are not fully consistent because of the different heights (model level vs elevation angle). Thus, the thresholds allowably differ slightly to highlight the structural similarities between the simulations and observations.

initial fields showed differences that can partially be attributed to the different horizontal resolutions of the original data. For example, regarding the wind fields, this structural difference resulted in a noisy bias field with a small-scale structure (not shown). Nevertheless, the wind fields at the initial date of our simulations (0600 UTC 9 June 2014) diverge slightly over northwestern France, where the first convective cell developed in our CCLM ERAI simulation (not shown). In the case of the specific humidity, we compared the precipitable water amount in the lower troposphere, and found higher values (about 20% 30% difference) in the ERA-Interim reanalysis over the development area of the Pentecost storm.

To determine the most important differences between the two distinct initial datasets, sensitivity studies were designed to identify those initial variables with the largest impact on the development of the storm in our simulations (see section 2). A considerable sensitivity was found when the initial specific humidity and wind fields were exchanged with ERA-Interim values in the ECMWF-analysis-driven simulation (Figs. 14c,d). By altering the specific humidity, the system intensified and the westerly displacement was reduced (cf. Figs. 14b and 14c). Nonetheless, two convective systems were simulated and merged together (Fig. 14c), which is in contrast to the real case. The consideration of the ERA-Interim horizontal wind fields also affected the development of the bow echo (Fig. 14d). A much better temporal and structural development of the storm compared to the CCLM AN simulation (Fig. 14b) is obvious, but still too far north. The exchanged wind fields actually lead to a

more distinct linear organization of the system when compared to the simulation with exchanged specific humidity (Fig. 14c). Simulations that consider the exchange of other initial variables (see section 2; Table 1) lead only to small variations of the resulting convective system (not shown). Based on the sensitivity studies, we assume that the representation of the wind and initial humidity fields is probably the key reason for a successful forecast of this storm event.

6. Summary and conclusions

A major linearly organized MCS developed on 9 June 2014 over Belgium and moved northeastward over western and northern Germany. It produced wind gusts of 25 40 m s ^{1} along an approximately 260-km-long path in the German federal state of NRW, where substantial damage occurred (Fig. 1). This Pentecost storm is classified as a bow echo as it shows the typical characteristics in the radar images: 1) a bow-shaped radar echo pattern; 2) a strong low-level reflectivity gradient; 3) a weak-echo region at the leading edge of the system; 4) a well-developed RIJ; 5) striking rear-inflow notches; and 6) a cyclonic bookend vortex. In addition, several overshooting tops were identified during the growth and mature phase of this severe bow echo.

The synoptic setting was very conducive to the development of this hazardous weather event. An overlap of areas with high amounts of boundary layer moisture, steep lower- to midtropospheric lapse rates, and strong deep-layer shear extended from southwestern France over Benelux to northern Germany, clearly depicting a large area with high potential for the occurrence of well-organized convective systems (Fig. 5). Moreover, the relatively strong midtropospheric flow and the parallelism of the average deep wind and shear vectors favored the formation of a severe wind-producing MCS. The convergence produced by the interaction of an outflow boundary from preexisting convection over northern France together with northeasterly winds over Belgium triggered uplift, thus leading to the initiation of the storm. The severe surface winds during the mature phase of the bow echo over western NRW occurred in association with the deep northern bookend vortex and the descending RIJ, which is in agreement with our simulations (Fig. 13) and other studies (e.g., Atkins et al. 2004; Wakimoto et al. 2006b; Weisman et al. 2013). Hence, we conclude that these two dynamic features of the bow echo contributed to the severe wind damage observed in the Rhine Ruhr region along the narrow straight-line swath (Fig. 1).

Our numerical experiments provide evidence that convection-permitting models are able to simulate bow echoes and their associated features. The ERA-Interim-driven CCLM simulation produced an MCS with a developing bow echo featuring similar mesoscale characteristics as those observed in reality (e.g., northern bookend vortex, midlevel RIJ, swath of severe winds). While the timing of the simulated storm coincides with the development of the observed system, the track of the simulated system was shifted northwestward by about 50 100 km. Sensitivity studies revealed that the bow echo formation is particularly sensitive to the wind field and the moisture content in the ambient environment and initial conditions, since they affect the strength of the storms' cold pool (James et al. 2006). In general, the initial and boundary conditions played a crucial role in the case of our simulations. This agrees also well with the work of Luo and Chen (2015), who made a similar analysis on an extreme-rain-producing MCS, and found that despite the favorable synoptic conditions the simulations were strongly sensitive to the initial conditions, especially to changes in moisture, wind, and temperature fields. An assessment of the forecasts also shows that most operational NWP models were not able to predict the Pentecost storm adequately in advance, despite the favorable ingredients (Fig. 12). Thus, our results suggest that initial and boundary conditions as well as other factors such as microphysical parameterizations (e.g., Adams-Selin et al. 2013; Barthlott et al. 2017) or data assimilation methods (e.g., Dixon et al. 2009; Lange and Craig 2014; Schwartz 2016) are highly significant in capturing similar extreme convective events properly.

The Pentecost storm was certainly one of the most violent thunderstorms in Germany in decades, and was comparable in size, intensity, and degree of organization to bow echo systems often observed over the United States. The investigation of such severe MCSs in Europe is very pertinent in light of the long-term climate change projections (Brooks 2013; Tippett et al. 2015), which suggest that while favorable meteorological conditions for the development of severe convective weather events over western Europe may occur more frequently in future decades, how the frequency of the various hazards will change is still an open question.

Acknowledgments. We thank the ECMWF for the provision of ERA-Interim and ECMWF analysis data, with a special thank you to Fernando Prates (ECMWF) for discussions regarding the differences between the NWP assimilation cycles. We thank the German Climate Computer Center (DKRZ, Hamburg) for computing and storage resources within the context of DKRZ project ANDIVA (No. 105). We thank Lars Kirchhübel and Markus Böhnke from the DWD for

providing access to the NinJo workstation, the replay server, and discussions. We are grateful to the European Severe Storm Laboratory (ESSL) for the reports taken from the European Severe Weather Database (ESWD; www.eswd.eu) shown in Fig. 1, and to Sebastian Keßler for GIS help regarding Figs. 2 and 14. FDK is funded by AON Benfield Impact Forecasting. JGP thanks the AXA Research Fund for support. Finally, we thank the three anonymous reviewers for their constructive comments that helped to improve the manuscript.

REFERENCES

Adams Selin, R. D., and R. H. Johnson, 2013: Examination of gravity waves associated with the 13 March 2003 bow echo. *Mon. Wea. Rev.*, **141**, 3735 3756, doi:10.1175/MWR D 12 00343.1.

, S. C. Van den Heever, and R. H. Johnson, 2013: Sensitivity of bow echo simulation to microphysical parameterizations. *Wea. Forecasting*, **28**, 1188 1209, doi:10.1175/WAF D 12 00108.1.

Atkins, N. T., J. M. Arnott, R. W. Przybylinski, R. A. Wolf, and B. D. Ketcham, 2004: Vortex structure and evolution within bow echoes. Part I: Single Doppler and damage analysis of the 29 June 1998 derecho. *Mon. Wea. Rev.*, **132**, 2224 2242, doi:10.1175/1520 0493(2004)132<2224:VSAEWB>2.0.CO;2.

, C. S. Bouchard, R. W. Przybylinski, R. J. Trapp, and G. Schmocker, 2005: Damaging surface wind mechanisms within the 10 June 2003 Saint Louis bow echo during BAMEX. *Mon. Wea. Rev.*, **133**, 2275 2296, doi:10.1175/MWR2973.1.

Baldauf, M., A. Seifert, J. Förstner, D. Majewski, and M. Raschendorfer, 2011: Operational convective scale numerical weather prediction with the COSMO model: Description and sensitivities. *Mon. Wea. Rev.*, **139**, 3887 3905, doi:10.1175/MWR D 10 05013.1.

Barthlott, C., and Coauthors, 2011: Initiation of deep convection at marginal instability in an ensemble of mesoscale models: A case study from COPS. *Quart. J. Roy. Meteor. Soc.*, **137**, 118 136, doi:10.1002/qj.707.

, B. Mühr, and C. Hoose, 2017: Sensitivity of the 2014 Pentecost storms over Germany to different model grids and microphysics schemes. *Quart. J. Roy. Meteor. Soc.*, doi:10.1002/qj.3019, in press.

Bedka, K. M., 2011: Overshooting cloud top detections using MSG SEVIRI infrared brightness temperatures and their relationship to severe weather over Europe. *Atmos. Res.*, **99**, 175 189, doi:10.1016/j.atmosres.2010.10.001.

Bennett, L. J., K. A. Browning, A. M. Blyth, D. J. Parker, and P. A. Clark, 2006: A review of the initiation of precipitating convection in the United Kingdom. *Quart. J. Roy. Meteor. Soc.*, **132**, 1001 1020, doi:10.1256/qj.05.54.

Betz, H. D., K. Schmidt, P. Laroche, P. Blanchet, P. Oettinger, E. Defer, Z. Dziewit, and J. Konarski, 2009: LINET An international lightning detection network in Europe. *Atmos. Res.*, **91**, 564 573, doi:10.1016/j.atmosres.2008.06.012.

Beyer, M., and H. Tuschy, 2015: A severe bow echo in western Germany on June 9, 2014: Forecasting and warning of a high impact weather event with the help of different tools and methods. *Eighth European Conf. on Severe Storms*, Wiener Neustadt, Austria, European Severe Storms Laboratory. [Available online at http://meetingorganizer.copernicus.org/ECSS2015/ECSS2015 114 2.pdf.]

Brooks, H. E., 2009: Proximity soundings for Europe and the United States from reanalysis data. *Atmos. Res.*, **93**, 546 553, doi:10.1016/j.atmosres.2008.10.005.

, 2013: Severe thunderstorms and climate change. *Atmos. Res.*, **123**, 129 138, doi:10.1016/j.atmosres.2012.04.002.

, J. W. Lee, and J. P. Craven, 2003: The spatial distribution of severe thunderstorm and tornado environments from global reanalysis data. *Atmos. Res.*, **67 68**, 73 94, doi:10.1016/S0169 8095(03)00045 0.

Brown, R. A., and V. T. Wood, 2007: A guide for interpreting Doppler velocity patterns: Northern Hemisphere edition. NOAA/National Severe Storms Laboratory, 55 pp. [Available online at https://www.nssl.noaa.gov/publications/dopplerguide/.]

Bryan, G., and M. Parker, 2010: Observations of a squall line and its near environment using high frequency rawinsonde launches during VORTEX 2. *Mon. Wea. Rev.*, **138**, 4076 4097, doi:10.1175/2010MWR3359.1.

Burgess, D. W., and B. F. Smull, 1990: Doppler radar observations of a bow echo associated with a long track severe windstorm. Preprints, *16th Conf. on Severe Local Storms*, Kananaskis Park, AB, Canada, Amer. Meteor. Soc., 203 208.

Chisholm, A. J., 1973: Radar case studies and airflow models. *Alberta Hailstorms*, *Meteor. Monogr.*, No. 36, Amer. Meteor. Soc., 1 36.

Clark, A. J., M. Xue, and F. Kong, 2009: A comparison of precipitation forecast skill between small convection allowing and large convection parameterizing ensembles. *Wea. Forecasting*, **24**, 1121 1140, doi:10.1175/2009WAF2222222.1.

Cohen, A. E., M. C. Coniglio, S. F. Corfidi, and S. J. Corfidi, 2007: Discrimination of mesoscale convective system environment using sounding observations. *Wea. Forecasting*, **22**, 1045 1062, doi:10.1175/WAF1040.1.

Coniglio, M. C., and D. J. Stensrud, 2001: Simulation of a progressive derecho using composite initial conditions. *Mon. Wea. Rev.*, **129**, 1593 1616, doi:10.1175/1520 0493(2001)129<1593:SOAPDU>2.0.CO;2.

, J. Y. Hwang, and D. J. Stensrud, 2010: Environmental factors in the upscale growth and longevity of MCSs derived from rapid update cycle analyses. *Mon. Wea. Rev.*, **138**, 3514 3539, doi:10.1175/2010MWR3233.1.

Corfidi, S. F., 2003: Cold pools and MCS propagation: Forecasting the maintenance of downwind developing MCSs. *Wea. Forecasting*, **18**, 997 1017, doi:10.1175/1520 0434(2003)018<0997:CPAMPF>2.0.CO;2.

Dee, D. P., and Coauthors, 2011: The ERA Interim reanalysis: Configuration and performance of the data assimilation system. *Quart. J. Roy. Meteor. Soc.*, **137**, 553 597, doi:10.1002/qj.828.

Deutsche Rück, 2015: Sturmdokumentation 2014 Deutschland. Deutsche Rückversicherung, Düsseldorf, Germany, 48 pp. [Available online at http://www.deutscherueck.de/fileadmin/user upload/Sturmdoku 2014 WEB.pdf.]

Dixon, M., Z. Li, H. Lean, N. Roberts, and S. Ballard, 2009: Impact of data assimilation on forecasting convection over the United Kingdom using a high resolution version of the Met Office Unified Model. *Mon. Wea. Rev.*, **137**, 1562 1584, doi:10.1175/2008MWR2561.1.

Doms, G., and Coauthors, 2011: A description of the nonhydrostatic regional COSMO model. Part II: Physical parameterization. Deutscher Wetterdienst, Offenbach, Germany, 154 pp. [Available online at http://www.cosmo model.org/content/model/documentation/core/cosmoPhysParamtr.pdf.]

Dotzek, N., P. Groenemeijer, B. Feuerstein, and A. M. Holzer, 2009: Overview of ESSL's severe convective storms research using the European Severe Weather Database ESWD. *Atmos. Res.*, **93**, 575 586, doi:10.1016/j.atmosres.2008.10.020.

Evans, J. S., and C. A. Doswell III, 2001: Examination of der echo environments using proximity soundings. *Wea. Fore casting*, **16**, 329 342, doi:10.1175/1520 0434(2001)016<0329: EODEUP>2.0.CO;2.

Fawbush, W. J., and R. C. Miller, 1952: A mean sounding repre sentative of the tornadic air mass environment. *Bull. Amer. Meteor. Soc.*, **33**, 303 307.

Fink, A. H., T. Brücher, V. Ermert, A. Krüger, and J. G. Pinto, 2009: The European storm Kyrill in January 2007: Synoptic evolution, meteorological impacts and some considerations with respect to climate change. *Nat. Hazards Earth Syst. Sci.*, **9**, 405 423, doi:10.5194/nhess 9 405 2009.

Fosser, G., S. Khodayar, and P. Berg, 2015: Benefit of convection permitting climate model simulations in the representation of convective precipitation. *Climate Dyn.*, **44**, 45 60, doi:10.1007/ s00382 014 2242 1.

Fujita, T. T., 1978: Manual of downburst identification for project NIMROD. Satellite and Mesometeorology Research Paper 156, Dept. of Geophysical Sciences, University of Chicago, 104 pp. [Available online at https://ntrs.nasa.gov/search.jsp? R 19780022828.]

Funk, T. W., K. E. Darmofal, J. D. Kirkpatrick, V. L. DeWald, R. W. Przybylinski, G. K. Schmocker, and Y. J. Lin, 1999: Storm reflectivity and mesocyclone evolution associated with the 15 April 1994 squall line over Kentucky and southern Indiana. *Wea. Forecasting*, **14**, 976 993, doi:10.1175/ 1520 0434(1999)014<0976:SRAMEA>2.0.CO;2.

Gatzen, C., 2004: A derecho in Europe: Berlin, 10 July 2002. *Wea. Forecasting*, **19**, 639 645, doi:10.1175/1520 0434(2004)019<0639: ADIEBJ>2.0.CO;2.

, 2013: Warm season severe wind events in Germany. *Atmos. Res.*, **123**, 197 205, doi:10.1016/j.atmosres.2012.07.017.

Helmert, K., and Coauthors, 2014: DWDs new radar network and post processing algorithm chain. *Eighth European Conf. on Radar in Meteorology and Hydrology*, Garmisch Partenkirchen, Germany, DWD DLR. [Available online at http://www.pa.op.dlr.de/erad2014/programme/ExtendedAbstracts/ 237 Helmert.pdf.]

Hengstebeck, T., D. Heizenreder, P. Joe, and P. Lang, 2011: The mesocyclone detection algorithm of DWD. *Sixth European Conf. on Severe Storms*, Palma de Mallorca, Spain, European Severe Storms Laboratory. [Available online at http://www. essl.org/ECSS/2011/programme/abstracts/196.pdf.]

, , and , 2014: Detection of atmospheric rotation by means of the DWD weather radar network. *Eighth Euro pean Conf. on Radar in Meteorology and Hydrology*, Garmisch Partenkirchen, Germany, DWD DLR. [Avail able online at http://www.pa.op.dlr.de/erad2014/programme/ ExtendedAbstracts/196 Hengstebeck.pdf.]

Houze, R. A., Jr., 1993: *Cloud Dynamics*. Academic Press, 573 pp.

, 2004: Mesoscale convective systems. *Rev. Geophys.*, **42**, RG4003, doi:10.1029/2004RG000150.

Irsic Zibert, M., B. Strajnar, and J. Zibert, 2010: Cold ring pattern on satellite images as indication of severe weather. *Proc. 2010 EUMETSAT Meteorological Satellite Conf.*, Cordoba, Spain, EUMETSAT. [Available online at https:// www.eumetsat.int/website/wcm/idc/idcplg?IdcService GET FILE&dDocName PDF CONF P57 S7 12 IRSICZIB V&RevisionSelectionMethod LatestReleased&Rendition Web.]

Jacobsen, I., and E. Heise, 1982: A new economic method for the computation of the surface temperature in numerical models. *Contrib. Atmos. Phys.*, **55**, 128 141.

James, R. P., P. M. Markowski, and J. M. Fritsch, 2006: Bow echo sensitivity to ambient moisture and cold pool strength. *Mon. Wea. Rev.*, **134**, 950 964, doi:10.1175/MWR3109.1.

Joe, P., H. J. Koppert, D. Heizenreder, B. Erbshäusser, W. Raatz, B. Reichert, and M. Rohn, 2005: Severe weather forecasting tools in NinJo. *Symp. on Nowcasting and Very Short Range Forecasting*, Toulouse, France, World Weather Research Programme, 7.13. [Available online at http://www.ninjo workstation.com/fileadmin/files/downloads/publications/Pub Joe Toulouse Severe Weather Forecasting.pdf.]

Johns, R. H., and C. A. Doswell III, 1992: Severe local storms forecasting. *Wea. Forecasting*, **7**, 588 612, doi:10.1175/ 1520 0434(1992)007<0588:SLSF>2.0.CO;2.

Johnson, R. H., and P. J. Hamilton, 1988: The relationship of surface pressure features to the precipitation and airflow structure of a midlatitude squall line. *Mon. Wea. Rev.*, **116**, 1444 1473, doi:10.1175/1520 0493(1988)116<1444:TROSPF>2.0.CO;2.

Kain, J. S., S. J. Weiss, J. J. Levit, M. E. Baldwin, and D. R. Bright, 2006: Examination of convection allowing configurations of the WRF Model for the prediction of severe convective weather: The SPC/NSSL Spring Program 2004. *Wea. Fore casting*, **21**, 167 181, doi:10.1175/WAF906.1.

Kühnlein, C., C. Keil, G. C. Craig, and C. Gebhardt, 2014: The impact of downscaled initial condition perturbations on convective scale ensemble forecasts of precipitation. *Quart. J. Roy. Meteor. Soc.*, **140**, 1552 1562, doi:10.1002/qj.2238.

Lange, H., and G. C. Craig, 2014: The impact of data assimilation length scales on analysis and prediction of convective storms. *Mon. Wea. Rev.*, **142**, 3781 3808, doi:10.1175/ MWR D 13 00304.1.

Lemon, L. R., 1980: Severe thunderstorm radar identification techniques and warning criteria. NOAA Tech. Memo. NWS NSSFC 3, 60 pp. [Available from NOAA/Central Library, 1315 East West Hwy., Silver Spring, MD 20910.]

Leutwyler, D., O. Fuhrer, X. Lapillonne, D. Lüthi, and C. Schär, 2016: Towards European scale convection resolving climate simulations with GPUs: A study with COSMO 4.19. *Geosci. Model Dev.*, **9**, 3393 3412, doi:10.5194/gmd 9 3393 2016.

Ludwig, P., J. G. Pinto, S. A. Hoepp, A. H. Fink, and S. L. Gray, 2015: Secondary cyclogenesis along an occluded front leading to damaging wind gusts: Windstorm Kyrill, January 2007. *Mon. Wea. Rev.*, **143**, 1417 1437, doi:10.1175/MWR D 14 00304.1.

Luo, Y., and Y. Chen, 2015: Investigation of the predictability and physical mechanisms of an extreme rainfall producing meso scale convective system along the Meiyu front in East China: An ensemble approach. *J. Geophys. Res. Atmos.*, **120**, 10 593 10 618, doi:10.1002/2015JD023584.

Lynch, P., 1997: The Dolph Chebyshev window: A simple opti mal filter. *Mon. Wea. Rev.*, **125**, 655 660, doi:10.1175/ 1520 0493(1997)125<0655:TDCWAS>2.0.CO;2.

Mikuš, P., and N. Strelec Mahović, 2013: Satellite based over shooting top detection methods and the analysis of correlated weather conditions. *Atmos. Res.*, **123**, 268 280, doi:10.1016/ j.atmosres.2012.09.001.

Morris, R., 1986: The Spanish plume Testing the forecaster's nerve. *Meteor. Mag.*, **115**, 349 357.

Nolen, R. H., 1959: A radar pattern associated with tornadoes. *Bull. Amer. Meteor. Soc.*, **40**, 277 279.

Parker, M. D., and R. H. Johnson, 2000: Organizational modes of midlatitude mesoscale convective systems. *Mon. Wea.*

Rev., **128**, 3413 3436, doi:10.1175/1520 0493(2001)129<3413:OMOMMC>2.0.CO;2.

Prein, A. F., and Coauthors, 2015: A review on regional convection permitting climate modeling: Demonstrations, prospects, and challenges. *Rev. Geophys.*, **53**, 323 361, doi:10.1002/2014RG000475.

Przybylinski, R. W., 1995: The bow echo: Observations, numerical simulations, and severe weather detection methods. *Wea. Fore casting*, **10**, 203 218, doi:10.1175/1520 0434(1995)010<0203:TBEONS>2.0.CO;2.

Púčik, T., P. Groenemeijer, D. Ryìva, and M. Kolaìř, 2015: Prox imity soundings of severe and nonsevere thunderstorms in central Europe. *Mon. Wea. Rev.*, **143**, 4805 4821, doi:10.1175/MWR D 15 0104.1.

Punkka, A. J., J. Teittinen, and R. H. Johns, 2006: Synoptic and mesoscale analysis of a high latitude derecho severe thun derstorm outbreak in Finland on 5 July 2002. *Wea. Fore casting*, **21**, 752 763, doi:10.1175/WAF953.1.

Ramis, C., J. Arus, and J. M. Lopez, 1997: Two cases of severe weather in Catalonia (Spain): An observational study. *Meteor. Appl.*, **4**, 207 217, doi:10.1017/S1350482797000510.

Rasmussen, E. N., and D. O. Blanchard, 1998: A baseline clima tology of sounding derived supercell and tornado forecast parameters. *Wea. Forecasting*, **13**, 1148 1164, doi:10.1175/1520 0434(1998)013<1148:ABCOSD>2.0.CO;2.

Ritter, B., and J. F. Geleyn, 1992: A comprehensive radiation scheme for numerical weather prediction models with potential appli cations in climate simulations. *Mon. Wea. Rev.*, **120**, 303 325, doi:10.1175/1520 0493(1992)120<0303:ACRSFN>2.0.CO;2.

Rockel, B., E. Raschke, and B. Weyres, 1991: A parameterization of broad band radiative transfer properties of water, ice, and mixed clouds. *Beitr. Phys. Atmos.*, **64**, 1 12.

, A. Will, and A. Hense, 2008: The regional climate model COMSO CLM (CCLM). *Meteor. Z.*, **17**, 347 348, doi:10.1127/0941 2948/2008/0309.

Schenkman, A. D., and M. Xue, 2016: Bow echo mesovortices: A review. *Atmos. Res.*, **170**, 1 13, doi:10.1016/j.atmosres.2015.11.003.

Schmetz, J., P. Pili, S. Tjemkes, D. Just, J. Kerkmann, S. Rota, and A. Ratier, 2002: An introduction to Meteosat Second Gener ation (MSG). *Bull. Amer. Meteor. Soc.*, **83**, 977 992, doi:10.1175/1520 0477(2002)083<0977:AITMSG>2.3.CO;2.

Schmid, W., H. H. Schiesser, M. Furger, and M. Jenni, 2000: The origin of severe winds in a tornadic bow echo storm over northern Switzerland. *Mon. Wea. Rev.*, **128**, 192 207, doi:10.1175/1520 0493(2000)128<0192:TOOSWI>2.0.CO;2.

Schmidt, J. M., and W. R. Cotton, 1989: A high plains squall line associated with severe surface winds. *J. Atmos. Sci.*, **46**, 281 302, doi:10.1175/1520 0469(1989)046<0281:AHPSLA>2.0.CO;2.

Schulz, J. P., and U. Schättler, 2014: Kurze Beschreibung des Lokal Modells Europa COSMO EU (LME) und seine Datenbanken auf dem Datenserver des DWD. Deutscher Wetterdienst, Offenbach, Germany, 81 pp. [Available online at https://www.dwd.de/SharedDocs/downloads/DE/modelldokumentationen/nwv/cosmo eu/cosmo eu dbbeschr 201406.pdf? blob publicationFile&v 3.]

Schwartz, C. S., 2016: Improving large domain convection allowing forecasts with high resolution analyses and ensemble data assimilation. *Mon. Wea. Rev.*, **144**, 1777 1803, doi:10.1175/MWR D 15 0286.1.

Setvák, M., and Coauthors, 2010: Satellite observed cold ring shaped features atop convective clouds. *Atmos. Res.*, **97**, 80 96, doi:10.1016/j.atmosres.2010.03.009.

Skamarock, W. C., M. L. Weisman, and J. B. Klemp, 1994: Three dimensional evolution of simulated long lived squall lines. *J. Atmos. Sci.*, **51**, 2563 2584, doi:10.1175/1520 0469(1994)051<2563:TDEOSL>2.0.CO;2.

Tiedtke, M., 1989: A comprehensive mass flux scheme for cu mulus parameterization in large scale models. *Mon. Wea. Rev.*, **117**, 1779 1800, doi:10.1175/1520 0493(1989)117<1779:ACMFSF>2.0.CO;2.

Tippett, M. K., J. T. Allen, V. A. Gensini, and H. E. Brooks, 2015: Climate and hazardous convective weather. *Curr. Climate Change Rep.*, **1**, 60 73, doi:10.1007/s40641 015 0006 6.

Trapp, R. J., and M. L. Weisman, 2003: Low level mesovortices within squall lines and bow echoes. Part II: Their genesis and implications. *Mon. Wea. Rev.*, **131**, 2804 2823, doi:10.1175/1520 0493(2003)131<2804:LMWSLA>2.0.CO;2.

Van Delden, A., 1998: The synoptic setting of a thundery low and associated prefrontal squall line in western Europe. *Meteor. Atmos. Phys.*, **65**, 113 131, doi:10.1007/BF01030272.

Wakimoto, R. M., H. V. Murphey, A. Nester, D. P. Jorgensen, and N. T. Atkins, 2006a: High winds generated by bow echoes. Part I: Overview of the Omaha bow echo 5 July 2013 storm during BAMEX. *Mon. Wea. Rev.*, **134**, 2793 2812, doi:10.1175/MWR3215.1.

, , C. A. Davis, and N. T. Atkins, 2006b: High winds generated by bow echoes. Part II: The relationship between the mesovortices and damaging straight line winds. *Mon. Wea. Rev.*, **134**, 2813 2829, doi:10.1175/MWR3216.1.

Wapler, K., T. Hengstebeck, and P. Groenemeijer, 2016: Mesocy clones in central Europe as seen by radar. *Atmos. Res.*, **168**, 112 120, doi:10.1016/j.atmosres.2015.08.023.

Warren, R., D. Kirshbaum, R. Plant, and H. Lean, 2014: A 'Boscastle type' quasi stationary convective system over the UK Southwest Peninsula. *Quart. J. Roy. Meteor. Soc.*, **140**, 240 257, doi:10.1002/qj.2124.

Weisman, M. L., 1993: The genesis of severe, long lived bow echoes. *J. Atmos. Sci.*, **50**, 645 670, doi:10.1175/1520 0469(1993)050<0645:TGOSLL>2.0.CO;2.

, and J. B. Klemp, 1982: The dependence of numerically simulated convective storms on vertical wind shear and buoyancy. *Mon. Wea. Rev.*, **110**, 504 520, doi:10.1175/1520 0493(1982)110<0504:TDONSC>2.0.CO;2.

, and C. A. Davis, 1998: Mechanisms for the generation of me soscale vortices within quasi linear convective systems. *J. Atmos. Sci.*, **55**, 2603 2622, doi:10.1175/1520 0469(1998)055<2603:MFTGOM>2.0.CO;2.

, and R. J. Trapp, 2003: Low level mesovortices within squall lines and bow echoes: Part I: Overview and dependence on environmental shear. *Mon. Wea. Rev.*, **131**, 2779 2803, doi:10.1175/1520 0493(2003)131<2779:LMWSLA>2.0.CO;2.

, and R. Rotunno, 2004: ''A theory for strong long lived squall lines'' revisited. *J. Atmos. Sci.*, **61**, 361 382, doi:10.1175/1520 0469(2004)061<0361:ATFSLS>2.0.CO;2.

, C. A. Davis, W. Wang, K. W. Manning, and J. B. Klemp, 2008: Experiences with 0 36 h explicit convective forecasts with the WRF ARW Model. *Wea. Forecasting*, **23**, 407 437, doi:10.1175/2007WAF2007005.1.

, C. Evans, and L. Bosart, 2013: The 8 May 2009 superderecho: Analysis of a real time explicit convective forecast. *Wea. Forecasting*, **28**, 863 892, doi:10.1175/WAF D 12 00023.1.

Wheatley, D. M., R. J. Trapp, and N. T. Atkins, 2006: Radar and damage analysis of severe bow echoes observed during BAMEX. *Mon. Wea. Rev.*, **134**, 791 806, doi:10.1175/MWR3100.1.